LBL--18451

DE85 C10636

HYDROTHERMAL CONDITIONS AND RESATURATION TIMES IN UNDERGROUND OPENINGS FOR A NUCLEAR WASTE REPOSITORY IN THE UMTANUM FLOW AT THE BASALT WASTE ISOLATION PROJECT

Karsten Pruess
Gudmundur Bodvarsson

Earth Sciences Division
Lawrence Berkeley Laboratory
University of California
Berkeley, California 94720

July 1982

This work was prepared and supported by the Basalt Waste Isolation Project (BWIP), Rockwell Hanford Operations, through the U.S. Department of Energy Contract No. DE-AC03-76SF00098.

SUMMARY

Numerical simulation techniques have been used to study heat flow and pore fluid migration in the near field of storage tunnels and canister storage holes in a proposed high-level nuclear waste repository in the Umtanum Basalt at the Basalt Waste Isolation Project site at Hanford, Washington. Particular emphasis was placed on evaluating boiling conditions in the host rock. Sensitivity studies were performed to determine the influence of variations in critical site-specific parameters which are not presently accurately known.

The results indicate that, even when rather extreme values are assumed for key hydrothermal parameters, the volume of rock dried by boiling of pore fluids is negligible compared to the volume of excavated openings. The time required for saturation of backfilling materials is thus controlled by the volume of the mined excavations. When realistic values for the parameters of the natural and man-made systems are used resaturation is predicted to occur within less than two years after backfilling is placed.

The approximations used in the analyses, and their limitations, are discussed in the body of the report. Recommendations are made for additional studies of the thermohydrological behavior of a high-level nuclear waste repository.

NOMENCLATURE

A: Area (L^2)

A_{nm}: Area of interface between volume elements n and m (L^2)

c_R: Specific heat of rock ($L^2/T^2 \cdot TEMP$)

d_{nm}: Distance between nodal points n and m (L)

D: Fracture spacing (L)

F_{nm}: Mass flux from volume element m into n (M/TL^2)

g_{nm}: Normal component of gravitational acceleration between volume elements n and m (L/T^2)

G_{nm}: Energy flux from volume element m into n (M/T^3)

h: Specific enthalpy (L^2/T^2) or heat transfer coefficient ($M/T^3 \cdot Temp$)

k: Superscript, indicates k^{th} time step

k: Absolute or intrinsic permeability (L^2)

k_β: relative permeability with reference to phase β (liquid, vapor); dimensionless

K: Heat conductivity ($M \cdot L/T^3 \cdot TEMP$)

p: Fluid pressure (M/LT^2)

q: Rate of mass production per unit volume (M/L^3T)

Q: Rate of energy production per unit volume (M/LT^3)

Qq_H: Heat flux per unit area (M/T^3)

q_n: Rate of mass production per unit volume from element n (M/L^3T)

Q_n: Rate of energy production per unit volume from element n (M/LT^3)

S_ℓ: Liquid saturation

$S_{\ell r}$: Irreducible liquid saturation

S_{Br}: Irreducible vapor saturation

t: Time (T)

T: Temperature (°TEMP)

T_r: Rock temperature (°TEMP)

T_{sr}: Temperature of storage room (°TEMP)

u: Specific internal energy of the fluid (L^2/T^2)

U: Internal energy contained in the rock-fluid mixture per unit volume of the medium (M/LT^2)

v, V: Volume (L^3)

V_n: Volume of element n (L^3)

μ: Viscosity (M/LT)

μ_β: Viscosity of phase b (M/LT)

ρ: Mass density (M/L^3)

ρ_R: Mass density of rock (M/L^3)

ρ_β: Mass density of b-phase (M/L^3)

Φ: Porosity

1.0 INTRODUCTION

A principal consideration in the design of a high-level nuclear waste repository is the heating of host rock and backfill due to radioactive decay of the material stored in the waste packages (canisters). Elevated temperatures may reduce the stability of the canister environment, and could accelerate the corrosion of the waste packages themselves. The hydrologic conditions at a repository site will have little impact on temperature transients if the rock mass permeability is very low. Nevertheless, even under conditions of low permeability, the interaction between hydrologic and thermal conditions must be carefully evaluated because (1) the presence of high-temperature, high-pressure steam around the waste packages may significantly alter corrosion and (2) some of the pore fluid in the vicinity of the repository can boil off, drying the near field rock mass. After repository backfilling and decommissioning, this dried rock mass and the backfill in storage rooms and canister storage holes represent unsaturated regions with pore fluid pressures much lower than prevailing groundwater pressure. Therefore, groundwaters in the vicinity of the repository would generally flow toward rather than away from the repository until all voids are saturated and pressurized. If the volume of dried rock is large, and resaturation is of long duration, the containment time for radio-nuclides may be enhanced, adding an additional margin of safety to overall repository performance.

Preliminary estimates of hydrothermal conditions in the vicinity of a high-level waste repository in the basaltic flows at the BWIP site have suggested that the resaturation time of the host rock that has been dried by boiling of pore fluid is approximately 300 years, while resaturation of the backfill in storage rooms and canister storage holes is approximately 3,000

years (Anderson, 1982). For the purpose of the preliminary scoping analyses, Anderson assumed that all of the rock mass which is heated to more than 100°C will be dried due to boiling. Based on this assumption, the zone of dried rock would extend some 20 meters radially around the axis of the waste canister. However, pore pressures at the BWIP reference repository location (RRL) at a depth of 3747.5 ft (1142.2 m) are expected to be close to 13 MPa. Pressures in the excavated openings will be reduced to atmospheric (0.1 MPa), but the presence of higher permeability zones above and below the entablature (within approximately 20 m of the repository) suggests that low pressures (~ 0.1 MPa) can be expected only in a very small region near the openings. The temperature required to initiate boiling will therefore be much higher than 100°C in most of the host rock, and the rock mass which is dry at the time of repository decommissioning will be correspondingly small.

In the preliminary estimates of repository resaturation described above Anderson assumed that groundwater flow toward the repository would be governed by the small regional hydraulic gradient. However, several orders of magnitude larger gradients and flows will result from the pressure sink generated by the excavation of underground openings. Resaturation will therefore occur much more rapidly than would be expected if gradients and flow rates were unperturbed.

The present study investigates drying and resaturation in the host rock, as well as resaturation in the backfill, in greater detail, taking spatial and temporal variations in temperatures and pressures into account. Geothermal reservoir simulation techniques were adapted to quantitatively model the interplay of heat conduction, fluid flow, and boiling and condensation

processes. The analyses have been made for the current conceptual repository design developed for the BWIP program. At the present stage of site characterization, several parameters required for the analyses are not accurately known. Values for these parameters were estimated in order to develop a reference case. These estimates were made in consultation with Rockwell's staff, from available site data, and the general literature. Studies have also been performed to investigate the sensitivity of the modeling results to a range of values for key parameters.

Significant approximations employed in the modeling work include (1) use of two-dimensional axisymmetric models, and (2) a porous medium approximation for the host rock. We believe that these approximations will have little influence on the principal conclusions of the study, which are (1) the volume of rock dried by steam formation is exceedingly small (less than 1 m^3 per canister); (2) resaturation of the dried rock volume is completed before the conceptual design calls for the underground openings to be backfilled (50 years); and (3) resaturation of the backfill occurs within less than two years after it is placed.

2.0 NUMERICAL SIMULATION OF FLUID AND HEAT TRANSPORT IN PERMEABLE ROCK MASSES

The simulations presented in this report were carried out with Lawrence Berkeley Laboratory's general purpose simulator MULKOM. MULKOM is an advanced version of the geothermal reservoir simulator SHAFT79 (Pruess and Schroeder, 1980). Both computer programs can model the flow of water/steam mixtures and heat in porous or fractured rock masses. The thermophysical properties of water substance are accurately represented by the steam table equations given by the International Formulation Committee (1967). The accuracy of MULKOM has been verified by comparison with a number of analytical solutions and by comparison with SHAFT79 calculations (Pruess and Narasimhan, 1982). SHAFT79, in turn, has been extensively verified both analytically and numerically (Stanford, 1980) and tested against data from geothermal fields (Pruess et al., 1980). MULKOM uses an integral finite difference method to solve the following mass and energy-balance equations:

$$\left(\phi_n^{k+1}\ \rho_n^{k+1} - \phi_n^k\ \rho_n^k\right) - \frac{\Delta t}{V_n}\left\{\sum_m F_{nm}^{k+1} A_{nm} + V_n q_n^{k+1}\right\} = 0 \qquad (2.1)$$

$$\left(U_n^{k+1} - U_n^k\right) - \frac{\Delta t}{V_n}\left\{\sum_m G_{nm}^{k+1} A_{nm} + V_n Q_n^{k+1}\right\} = 0 \qquad (2.2)$$

The subscript n labels the volume elements into which the system under study is partitioned, k labels the time step, and the other symbols are explained in the nomenclature.

The volumetric internal energy is a sum of fluid and rock contributions:

$$U = \phi\rho u + (1-\phi)\rho_r c_R T \qquad (2.3)$$

Mass flux is given by Darcy's Law, which, in discretized form, is written:

$$F_{nm} = \sum_{\substack{\beta=\text{liquid,}\\ \text{vapor}}} \left(\frac{k\, k_\beta}{\mu_\beta}\right)_{nm} \left(\rho_\beta\right)_{nm} \left[\frac{P_m - P_n}{d_{nm}} - \left(\rho_\beta\right)_{nm} g_{nm}\right] \qquad (2.4)$$

The quantities with subscripts "nm" are evaluated at the interface between volume elements n and m, using appropriate weighting procedures. The relative permebility k_β (β = liquid, vapor) assumes values between 0 and 1. It describes the impediment to flow of one phase due to the presence of the other phase in a two-phase system. Steam-water relative permeabilities are not well known at the present time, and there are indications that different parameterizations are applicable for different types of porosity (e.g. intergranular, fractures). We assume a linear relationship between relative permeability and phase saturation, as is often done for fractured rock masses:

$$k_{\beta=\text{liquid}} = \begin{cases} \dfrac{1-S_{lr}-S}{1-S_{lr}} & \text{for } S < 1-S_{lr} \\ 0 & \text{for } S > 1-S_{lr} \end{cases} \qquad (2.6)$$

$$k_{\beta=\text{vapor}} = \begin{cases} \dfrac{S-S_{sr}}{1-S_{sr}} & \text{for } S > S_{sr} \\ 0 & \text{for } S < S_{sr} \end{cases} \qquad (2.7)$$

Heat flux has a conductive and an advective component:

$$G_{nm} = K_{nm} \frac{T_m - T_n}{d_{nm}} + \sum_\beta \left(h_\beta\right)_{nm} \left(F_\beta\right)_{nm} \qquad (2.8)$$

The mass and energy balance equations are highly non-linear and strongly coupled. MULKOM solves all equations simultaneously, using Newton/Raphson iteration and a direct solution technique. The linear equations arising at

each iteration step are solved directly with the Harwell solver "MA28" which features a sparse version of Gaussian elimination (Duff, 1977).

The integral finite difference method (IFD) used in MULKOM is applicable to one-, two-, and three-dimensional systems with regular or irregular grid blocks. The geometric flexibility of the IFD method makes it possible to model naturally fractured flow systems by means of the technique of multiple interacting continua ("MINC"; Pruess and Narasimhan, 1982). However, the computational effort required for 3-D or fractured medium calculations is large and two-dimensional porous medium approximations were employed throughout the present study.

3.0 CONCEPTUAL REPOSITORY DESIGN AND MODELING APPROACH

3.1 Conceptual Repository Design

The reference conceptual design assumes that the repository will be constructed in the center of the Umtanum entablature at a nominal depth of 3747.5 ft (≅ 1142.2m, see Section 4). The entablature has a nominal thickness of 125 ft (≅ 38.1m), with higher permeability strata above and below. The repository layout is shown in Figure 3.1. For the present study it is sufficient to consider only a room-scale section (Figure 3.2). The storage rooms are parallel and separated by a distance of 61.0 m (pillar width). Neighboring rooms are connected by circular canister storage holes of 0.686 m diameter, spaced at a pitch of 32.6 m along the walls. Each storage hole holds 17 waste canisters. The canister arrangement is shown in more detail in Figure 3.3. Current plans are to leave the air spaces around canisters and the storage rooms open for 50 years, after which time backfill will be placed.

3.2 Symmetry Element

Because the canister holes on either side of the storage rooms are arranged in a staggered pattern (Figure 3.2), the repository symmetry is very inconvenient from the view point of numerical modeling. The basic symmetry element contains half of each of two off-center canister holes, with a section of the storage room in between. The flow geometry in the symmetry element is three-dimensional, and it does not lend itself readily for an approximation of less dimensions.

Three-dimensional simulations require a large computational effort. Test calculations showed that the requirements of the present study (fine

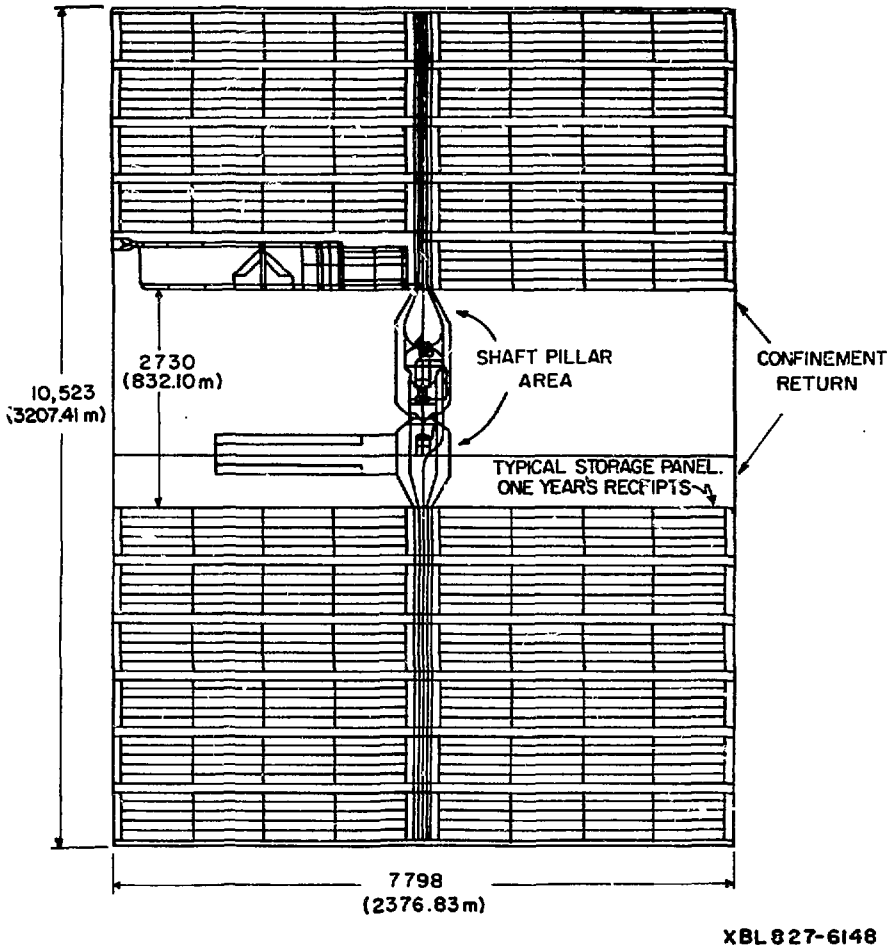

FIGURE 3.1 Repository layout (conceptual design).

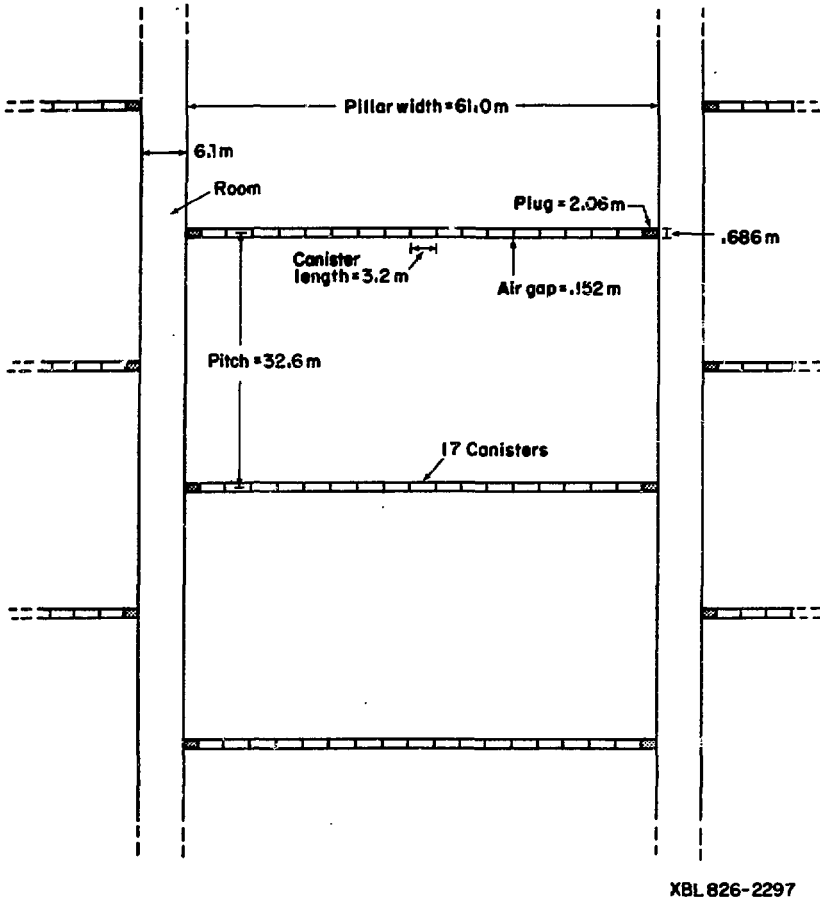

FIGURE 3.2 Layout of storage tunnels and canister storage holes (conceptual design).

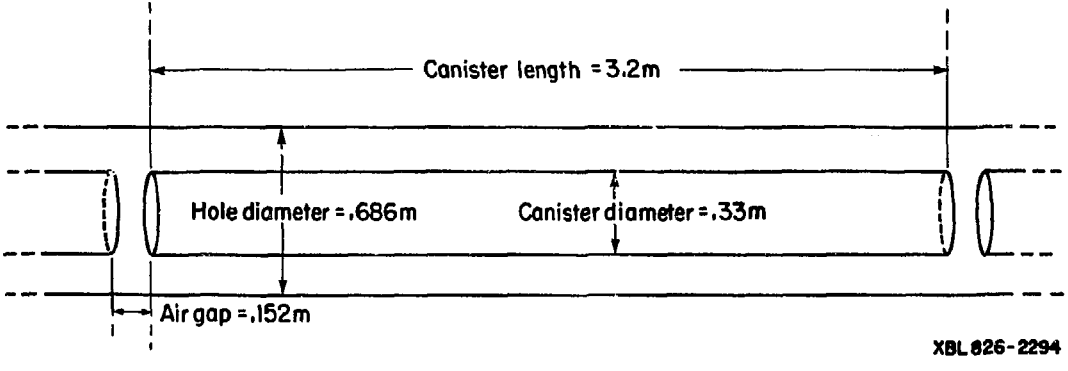

FIGURE 3.3 Arrangement of canisters in storage holes.

spatial resolution near storage rooms and canister holes, extended simulation times, and sensitivity analysis for key parameters) could not be met by three-dimensional calculations. Therefore, a modification of the conceptual design was developed* which would have little impact upon hydrothermal conditions, yet would more readily permit a less-than-three-dimensional approximation to be used.

The desired simplfication can be obtained by ignoring the displacement of the canister holes on one side of a storage tunnel relative to those on the other side, i.e., the canister holes are aligned opposite one another (Figure 3.4). In this modified pattern, all other dimensions are preserved. We believe that this geometrical modification will have a small impact upon the results of the computations. The main effect will be that slightly higher temperatures will be predicted for the region of the tunnel walls near the storage hole plugs, due to cumulative heating from the canisters on opposite sides of the storage room. This will tend to make the two-phase zone in the rock mass slightly larger than it would be if the repository were laid out as shown in Figure 3.2.

The modified layout shown in Figure 3.4, which for a "room-scale" problem can be considered to continue indefinitely in all directions, has a symmetry element which is bounded by vertical planes with "no flow" boundary conditions (Figure 3.5). Therefore, in the modeling effort only this element needs to be considered. Flow geometry within the symmetry element is still three-dimensional, but a two-dimensional approximation can easily be made.

*Modification was agreed in a meeting between Rockwell, LBL, and KE/PB in Oakland June 2, 1982.

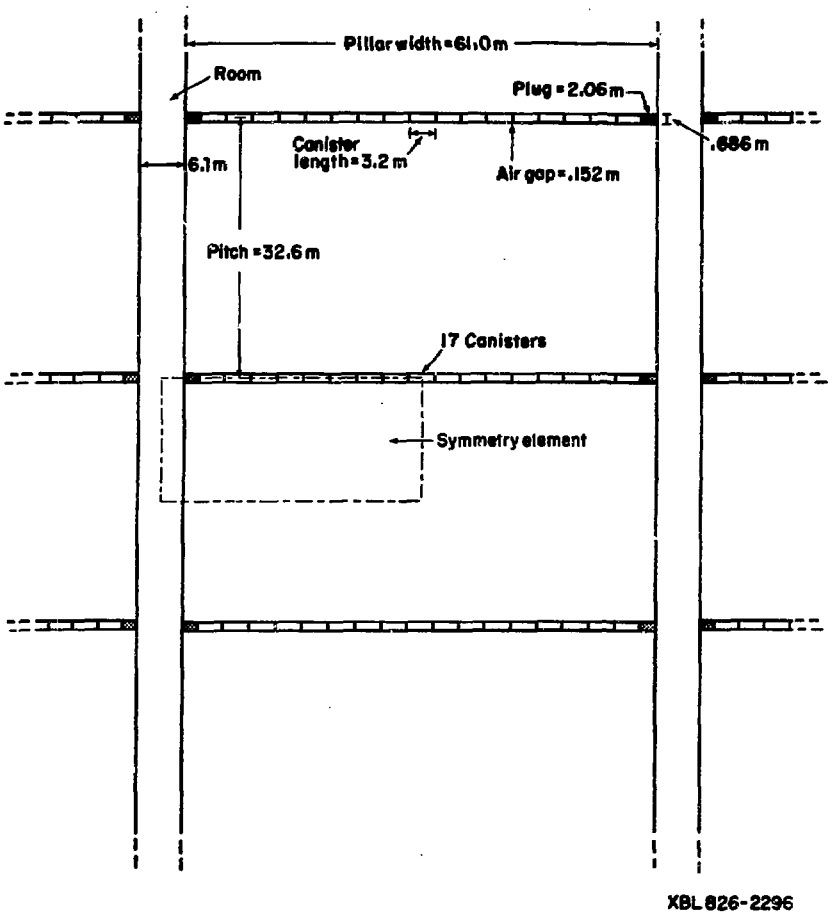

FIGURE 3.4 Modified room scale layout assumed for the numerical simulations.

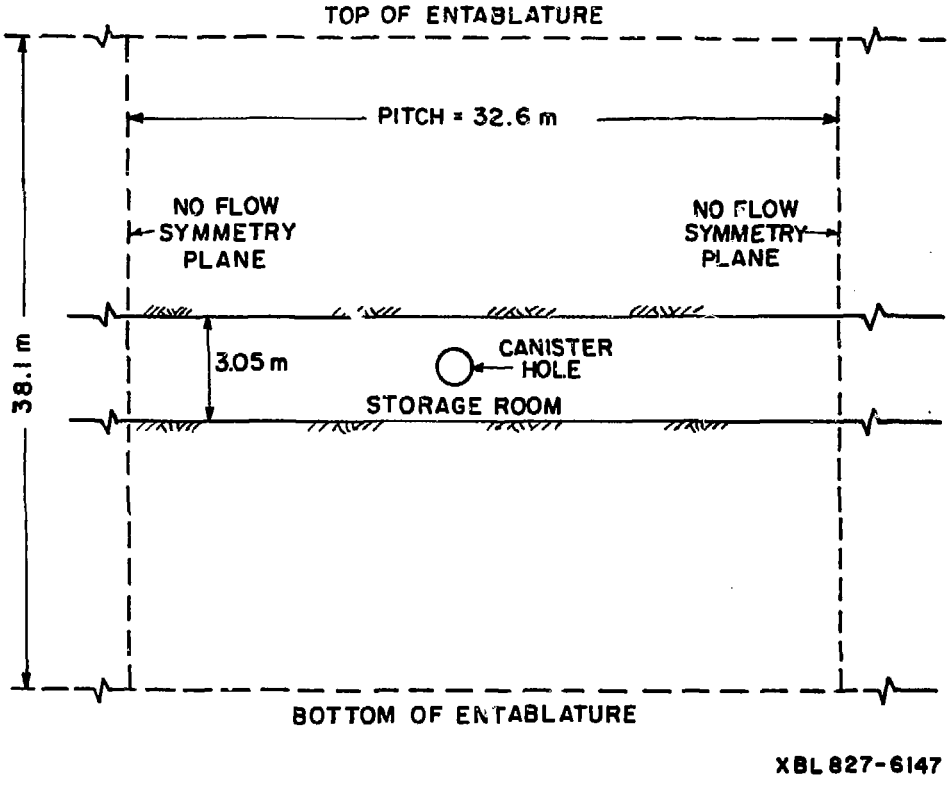

FIGURE 3.5 Sideview of the basic symmetry model used in the numerical simulations.

3.3 Axisymmetric Model

The hydrothermal regime is cylindrical in the near field of the canister storage hole, where the largest heat and fluid fluxes occur. The cylindrical symmetry is broken by the storage room, the upper and lower planar boundaries of the entablature, and the vertical symmetry planes between storage rooms (Figure 3.5). For the numerical simulations, the system shown in Figure 3.5 was approximated by the two-dimensional axisymmetric system shown in Figure 3.6.

In the development of the two-dimensional axisymmetric model, careful consideration was given to preserving important geometric parameters and to adequate representation of the appropriate boundary conditions. As shown in Figure 3.6, the outer radius of the axisymmetric system was taken as R = 19.89 m, in order to preserve the total cross sectional area. The cylinder length was taken equal to the actual system length, which is half the sum of the storage tunnel width and the pillar width. Therefore, total system volume is rigorously preserved. The conditions of the outer radius of the cylindrical system (Figure 3.6) must represent both the no-flow (vertical) boundaries, as well as the constant pressure boundaries assumed at the top and bottom of the entablature. To properly model these boundary conditions, the interface area between the cylinder and the surrounding constant pressure region was set equal to half the sum of the areas of the top and bottom boundaries of the entablature.

The canister storage hole can be represented rigorously in the axisymmetric model; but the geometry of the storage tunnel had to be extensively modified. The important quantities that must be preserved are the room

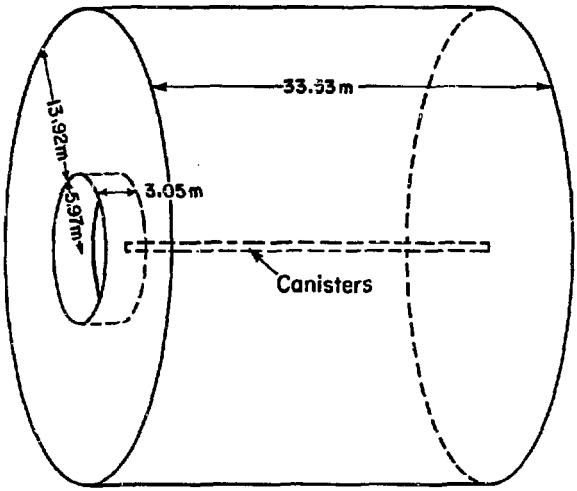

FIGURE 3.6 Schematic representation of the two-dimensional axisymmetric model.

width and total room wall area; both parameters will have a major impact on fluid and heat transport into the room. The shape of the room was changed from its tubular configuration to a disk. Because both the tunnel width and room wall area are preserved, room volume is increased from its actual value of 258.3 m^3 (per 8.5 canisters) to 341.5 m^3 in the axisymmetric model shown in Figure 3.6. However, in the numerical calculations, the volume of the disk representing the room is prescribed as the actual volume.

While the axisymetric approximation is accurate near the canister hole, and can be made to adequately represent conditions at the outer boundaries, there is a rather severe modification of the flow geometry in the vicinity of the room. The principal difference from the prototype is that most of the room wall area is located close to the canisters. Therefore, both conductive heat flow and fluid flow into the room from the rock near the canister storage holes will be overestimated while flow at larger distance from the canister will be underestimated. As a result, the axisymetric model will predict somewhat lower temperatures and pressures in the vicinity of the canister than would be obtained in a 3-D model.

The modification of the conceptual design into an axisymmetric model will result in some differences in predicted repository performance. In our judgement, these differences are minor relative to the uncertainties in site specific parameters. Similar approximations are commonly used in engineering analyses of complex underground structures, and have been applied in a recent analysis of the thermohydrologic performance of high-level nuclear waste repositories (Eaton and Reda, 1981).

Treatment of the air-filled spaces in the canister storage hole and storage tunnel also required simplifying approximations. Explicit distinction between the air and water components would have caused a great increase in the computational effort and is not necessary in our view. We believe that the behavior of the system can be quite accurately represented in terms of a single component water/steam mixture. In our model, the air filled spaces are treated as containing steam at initial temperatures of 27°C in the storage tunnels, and 300°C in the canister storage holes. The major inaccuracy introduced by this approximation is that room pressure is below atmospheric, namely, equal to the saturation pressure of water at 27°C (0.036 bars). This may appear to be a rather gross misrepresentation of room pressure, however, when compared to the reference formation pressure of 130 bars at repository depth, the overall pressure drop is changed by only 0.7% (from 129 to 129.964 bars). Therefore the effects on computed fluid flow will be negligible.

In the actual repository, the rooms will contain moist, quiescent air as well as some liquid water. The rooms will be closed off with bulkheads which are not hermetically sealed so that the pressure, before backfilling, is maintained at 1 bar. In the numerical model, room pressure remains below 1 bar until a temperature of 100°C is reached. After the room has heated to above 100°C, fluid entering the room is permitted to discharge into a pressure sink maintained at 1.0 bar.

3.4 Meshes Used in the Simulations

To perform numerical calculations, the axisymmetric model (Figure 3.6) must be descritized into a set of volume elements, or "mesh". In the analysis

we use two meshes, a fine mesh and a coarse mesh, depending upon the resolution required (see Section 5). The meshes consist of 10 layers bounded by planes oriented normal to the axis of the canisters. In the radial direction the elements are formed by concentric cylinders. A section through the coarse mesh is shown on Figure 3.7. For the coarse mesh, the model was divided into seven radial elements; while ten radial elements were used for the fine mesh. The locations of the boundaries of the layers and radial elements, and their thicknesses, are given in Tables 3.1 and 3.2 for the fine and coarse mesh, respectively.

We note that the first radial element in either mesh extends to the wall of the canister hole, representing both waste package and surrounding void space. While the heat flux leaving the canisters is properly represented, the detailed heat transfer mechanisms in the void space between canister and rock are not considered in our model. Therefore, predictions for rock temperatures will be reliable, but canister temperatures may be less accurate.

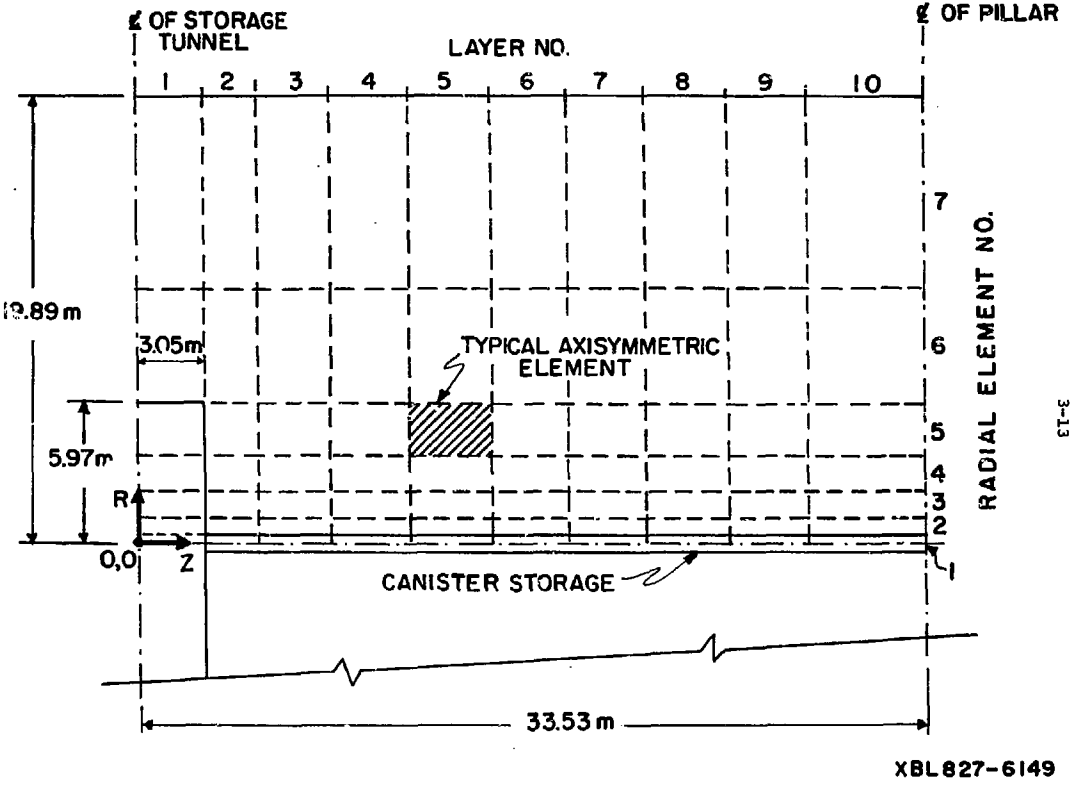

FIGURE 3.7 Discretization of model into axisymmetric elements (coarse mesh).

Table 3.1 Fine mesh for 2-D model.

Radial Elements	ΔR (M)	Cumulative Radius(M)	Layers	Thickness (M)	Cumulative Thickness(m)
1	0.343	0.343	1	3.048	3.048
2	0.044	0.387	2	2.057	5.105
3	0.088	0.475	3	3.277	8.382
4	0.177	0.652	4	3.353	11.735
5	0.354	1.006	5	3.353	15.088
6	0.710	1.716	6	3.353	18.440
7.	1.420	3.136	7	3.353	21.793
8	2.835	5.971	8	3.353	25.146
9	4.639	10.610	9	3.353	28.499
10	9.278	19.888	10	5.029	33.528

Table 3.2 Coarse mesh for 2-D model.

Radial Elements	ΔR (M)	Cumulative Radius(M)	Layers	Thickness (M)	Cumulative Thickness(m)
1	0.343	0.343	1	3.048	3.048
2	0.652	0.995	2	2.057	5.105
3	1.010	2.006	3	3.277	8.382
4	1.558	3.563	4	3.353	11.735
5	2.408	5.971	5	3.353	15.088
6	4.709	10.680	6	3.353	18.440
7.	9.208	19.888	7	3.353	21.793
			8	3.353	25.146
			9	3.353	28.499
			10	5.029	33.528

4.0 PARAMETERS USED IN THE NUMERICAL MODELS

4.1 Stratigraphy of the Hanford Basalts

The Columbia river basalts at the Hanford site consist of a sequence of flows. The principal formations at the reference repository location are the Saddle Mountains, Wanapum, and the Grande Ronde (Figure 4.1). Individual basalt flows are subdivided into one, or more, of the intra-flow structures shown in Figure 4.2. The physical characteristics of these flow structures may be described as:

1) Flow top--a thin layer of potentially weathered, scoriaceous lava and rubble, over a thicker layer of very vesicular lava;
2) Upper colonnade--a region containing large warped or twisted vertical hexagonal columns which may be 2 to 3 meters in diameter. Some cross-fracturing occurs and frequently coincides with horizontal elliptical vesicles;
3) Entablature--an intermediate zone characterized by slender columns which seem to form fan, or radiating, joint patterns. Large columns in the upper colonnade may continue in the entablature as bundles of small hexagonal columns;
4) Lower colonnade--a zone, sharply divided from the entablature, containing long symmetrical hexagonal columns formed by a regular pattern of vertical joints (Isherwood, 1980, Agapito, 1977).

4.2 Characteristics of the Umtanum Flow

The Umtanum basalt flow (Flow No. 9 of the Grande Ronde formation), in the Schwona sequence, has been designated as a reference horizon for the Basalt Waste Isolation Project. It is located at an approximate depth of 1142 m (Figure 4.3). It has a relatively thick entablature (on the average,

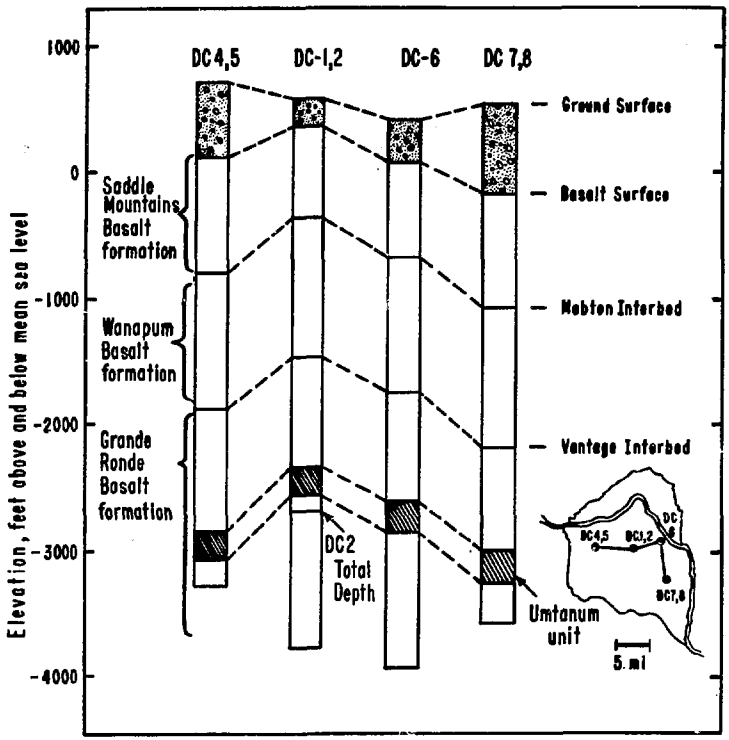

FIGURE 4.1 Basalt formations at the Hanford site.

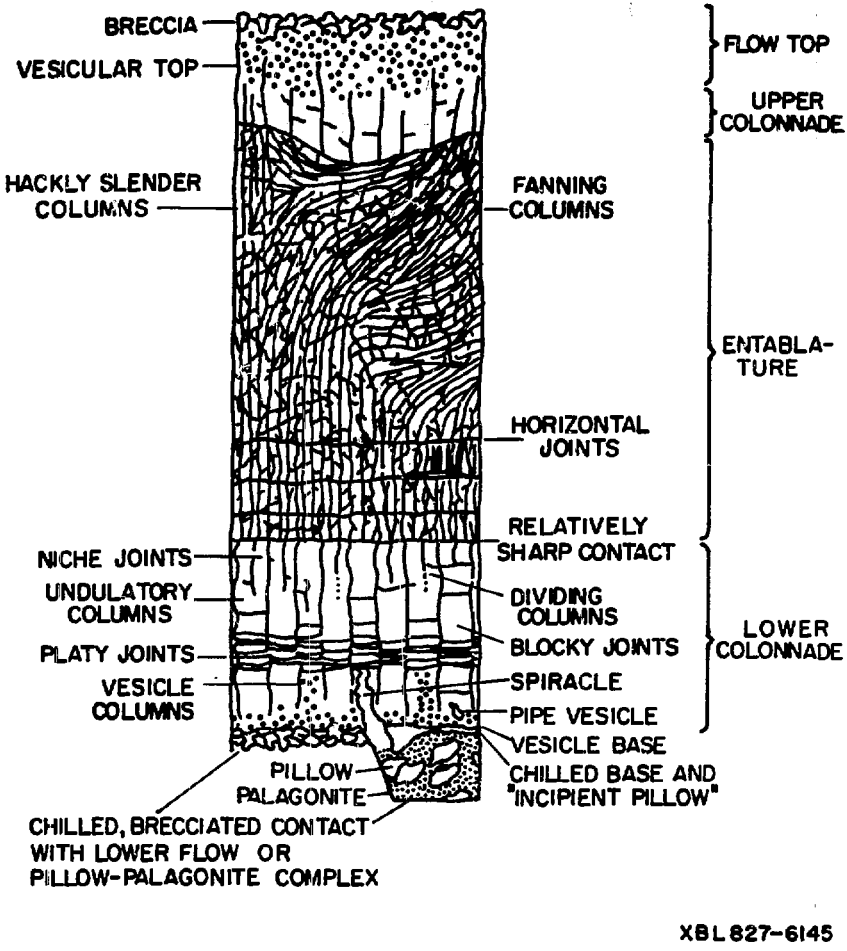

FIGURE 4.2 Schematic showing structure of basalt flow (modified from Atlantic Richfield Hanford Company, 1975).

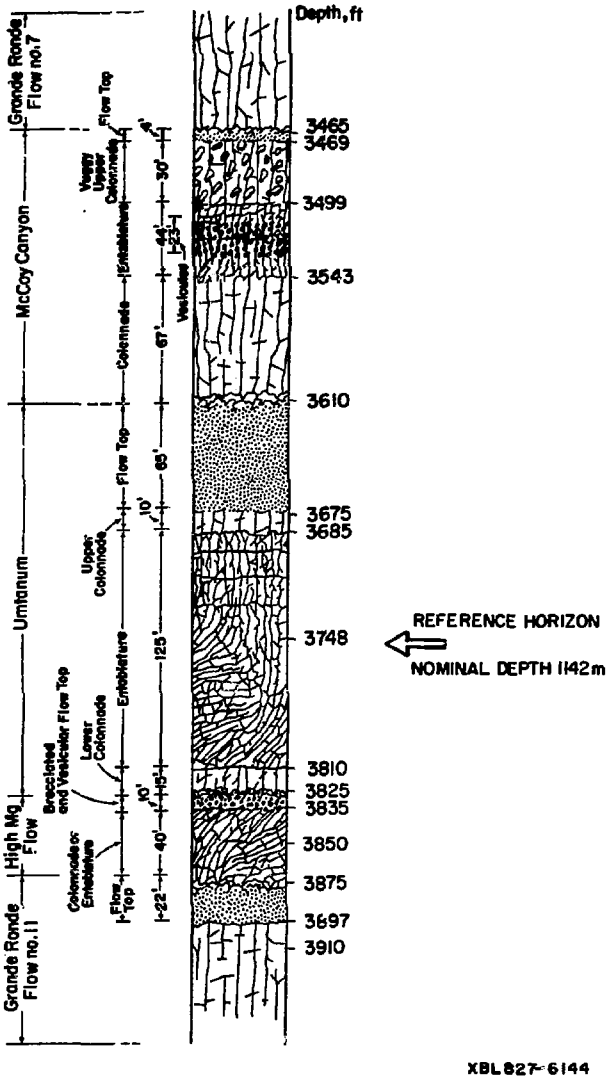

FIGURE 4.3 Location of reference horizon in the Umtanum.

38 m), which appears to be rather continuous laterally. For these reasons, it is being considered as a host rock for a nuclear waste repository (Schmidt et al., 1980).

The upper and lower colonnades of the Umtanum vary greatly in thickness (Myers and Price, 1981). In some of the holes drilled at the Hanford site these units were not found. Because of the irregularity of these units, they were not modelled in detail in the numerical simulations described in the present study.[1] Preliminary simulation studies have confirmed that specific consideration of the colonnade zones does not significantly change the results of the numerical analyses.

The flow top is relatively thick in the Umtanum unit (Figure 4.3). Its structural characteristics suggest that its permeability exceeds that of the entablature by several orders of magnitude (King et al., 1981).

4.3 Hydrologic and Thermomechanical Parameters

The material properties of the Umtanum's entablature layer are of primary interest in the present study. The material properties of the backfill material are needed for the resaturation calculations. In addition, the properties of the concrete plug, located in the ends of the canister storage holes, and the thermal properties of the air in the storage room are required for the simulation studies.

We have determined a base value for each of the parameters to be used in the calculations of a reference case. However, at the present time, many of

---

[1] This approach was agreed upon in a meeting between Rockwell and LBL staff held in Berkeley on March 9, 1982.

the key parameters are not accurately known; for these parameters we have determind a reasonable range of values for sensitivity studies.

The parameter values used for the reference case are given in Table 4.1 and the range of values estimated for the site is given in Table 4.2. In determining appropriate values and ranges for the model parameters we used data available in the general literature, reports of investigations conducted at the BWIP site, and recommendations provided by Rockwell. A brief discussion of each of the model parameters is given below.

4.3.1 Properties of the Umtanum Entablature Rock

4.1.1.1 Permeability. Horizonal permeability values of basalt flows in the Columbia River basalt group have been reported by Raymond and Tillson (1968); La Sala and Doty (1971); Deju and Fecht (1974); Apps et al. (1978); Gephart et al. (1978); Science Applications, Inc. (1978); Summers et al., (1978); and others. The most frequently reported hydraulic conductivity (permeability) values range from 10^{-7} to 10^{-11} m/s (10^{-14} to 10^{-18} m^2) for interflows, and from 10^{-11} to 10^{-14} m/s (10^{-18} to 10^{-21} m^2) for columnar basalt (Gephart et al., 1979b). The permeability values were calculated based on a water density of 1000 kg/m^3. No measurements of vertical permeability are currently available (KE/PB, 1982).

The horizontal and vertical permeabilities of the Umtanum entablature have been estimated as 10^{-11} m/s (10^{-18} m^2) and 10^{-10} m/s (10^{-17} m^2), respectively (King et al., 1981). These values are used for the reference case simulations (Table 4.1). King et al. estimate that these values are accurate to within one to two orders of magnitude. This information guided the range of permeabilities given in Table 4.2.

Table 4.1. Model parameters used for the reference case.

Parameter	Umtanum	Canisters Hole Plug	Backfill		Air in Storage Tunnel
			Canisters Storage Hole	Storage Tunnel	
Horizontal Permeability (m^2)	1.0×10^{-18}	∞	1.0×10^{-16}	1.0×10^{-15}	--
Vertical Permeability (m^2)	1.0×10^{-17}	∞	1.0×10^{-16}	1.0×10^{-15}	--
Porosity	0.001	0.20	0.25	0.50	1.0
Thermal Conductivity (J/m·s·°C)	2.30	1.37	0.75	0.75	--
Specific Heat (J/kg ·°C)	953.0	880.0	910.0	910.0	1005.0
Density (kg/m^3)	2780.0	2100.0	2100.0	2100.0	1.18
Compressibility (pa^{-1})	0.0	0.0	0.0	0.0	0.0
Heat Transfer Coefficient ($W/m^2 \cdot °C$)	--	--	--	--	25.0
Initial Water Content (by weight)	--	--	12%	12%	--
Coefficient of Thermal Expansion ($°C^{-1}$)	0.0	0.0	0.0	0.0	0.0

Table 4.2. Range of values for site-specific parameters.

Parameter	Umtanum Rock Mass	Backfill		Air in Storage Tunnel
		Canisters Storage Hole	Storage Tunnel	
Horizontal Permeability (m^2)	10^{-17} - 10^{-20}	10^{-15} - 10^{-17}	10^{-13} - 10^{-17}	--
Vertical Permeability (m^2)	10^{-17} - 10^{-20}	10^{-15} - 10^{-17}	10^{-13} - 10^{-17}	--
Porosity	0.0005 - 0.01	0.10 - 0.50	0.20 - 0.50	--
Thermal Conductivity (J/m s °C)	1.2 - 2.3	0.50 - 1.0	0.5 - 1.0	--
Specific Heat (J/kg °C)	920-1000	850 - 1000	850 - 1000	--
Density (kg/m^3)	2700-2820	1800 - 2300	1800 - 2300	--
Compressibility (pa^{-1})	0.0	0.0	0.0	--
Heat Transfer Coefficient (W/m^2 °C)	--	--	--	10 - 50
Initial Water Content (by weight)	--	8-20%	8-20%	--
Coefficient of Thermal Expansion ($°C^{-1}$)	0.0	0.0	0.0	0.0

4.3.1.2 Porosity. Porosity values for the Columbia River Basalt Group have been reported by La Sala and Doty (1971); Apps et al. (1978); Gephart et al. (1979); KE/PB (1980); FSI (1980b, 1981), King et al. (1981); and others. In general, the ranges of values quoted are 0.1 - 10% and 0.01 - 2% for the total and apparent porosities, respectively. For the Umtanum Entablature, Anderson (1982) reported a value of 0.1%, which was used in the reference case calculations (Table 4.1). Based on the values reported in the literature, a range of 0.0005 to 0.01 was selected for the porosity of the entablature (Table 4.2).

4.3.1.3 Thermal Conductivity. Measured thermal conductivities of the Hanford basalt flows have been reported by Agapito et al. (1977); CSM (1978); Martinez-Baez and Amick (1978); Schmidt et al. (1980); PSI (1980a, 1980b, and 1981); King et al. (1981); and others. Test results show that thermal conductivity increases with temperature. KE/PB (1980) give a correlation in the form:

$$K = 0.763 + 0.00389\ T(°C) \qquad (4.1a)$$

where T is the temperature of the rock and K is thermal conductivity, given in units of W/m°C. This correlation (Eqn 4.1a) was also cited by Anderson (1982), and was initially used in the present studies. However, at Rockwell's request, a different correlation was used in the for the reference case simulations presented here.[2] This correlation has the form:

$$K = 2.16 + 0.00075\ T(°C) \qquad (4.1b)$$

Therefore, for the reference case simulations, a value of K = 2.30 W/m°C (corresponding to an average rock temperature of 200°C) was used (Table 4.1).

---

[2] Letter from D. Turner (Rockwell) to D.J. Watkins (LBL) dated April 27, 1982. Rockwell Reference No., R82-1274

In determining an appropriate range for the thermal conductivity, the FSI (1981) data for the Umtanum entablature rock was used. The thermal conductivity values reported by FSI are for specimens from boreholes DH-5 and DC-2, tested over a temperature range of 100-300°C. The corresponding range in the thermal conductivity is 1.2 - 2.1 W/m°C. A similar range is given in Table 4.2, where the thermal conductivity value used in the reference case is the upper limit.

4.3.1.4 Specific Heat. Specific heat values (c_r) for Umtanum and Esquatzel basalts have been measured by Martinez-Baez and Amick (1978); Miller (1978a and 1978b); Miller and Bishop (1979); Erickson and Krupka (1980); and FSI (1980a and 1980b). They found that the specific heat of these basalts is somewhat temperature dependent. Schmidt et al. (1980) summarized the data and recommended the use of the correlation:

$$c_r = 837 + 0.837T(°C) \quad (4.2a)$$

where c_r is given in J/kg°C. This expression is based on an average density of 2830 kg/m^3. FSI (1981) performed laboratory tests to measure the specific heat of Umtanum entablature specimens. These, and other data, have been used to establish the most current correlation:[3]

$$c_r = 930 + 0.234T°C \quad (4.2b)$$

For the reference case, this latter correlation was used to determine the specific heat (Table 4.1). The range of values shown in Table 4.2 is based on the results reported by FSI (1981).

---

[3] Ibid.

4.3.1.5 Rock Density. Hanford basalt rock density has been measured by CSM (1978); Miller (1979a and 1979b); Miller and Bishop (1979); FSI (1980a, 1980b, and 1981); and others. These studies show that the average bulk density of the entablature of the Umtanum basalts is 2780 kg/m^3, with a range of 2580-2820 kg/m^3 (FSI, 1980b).

4.3.1.6 Rock Compressibility and Thermal Expansion. The effects of rock compressibility and thermal expansion were neglected in the present simulation studies (Tabels 4.1 and 4.2). The rock compressibility at repository depth (~ 1150 meters) is estimated to be at least an order of magnitude lower than the compressibility of the pore water. Similarly, studies of thermal expansion of the basalt flow report low values on the order of 6 x 10^{-6}°C^{-1} (Agapito et al., 1977; CSM, 1978; FSI, 1980a, 1980b, and 1981; and Erickson and Krupka, 1980). We believe that neglecting these parameters will have negligible effect on the results.

4.3.2 Properties of Backfill Materials

Current proposals for backfilling the storage tunnels and canister storage holes call for a basalt-bentonite mixtures. The properties of these mixtures are not yet well defined (Anderson, 1982), and depend greatly on the water content and the degree of compaction. Compositions being considered for the basalt/bentonite mixtures are 85/15 and 75/25 by weight, for the storage room and the canister hole, respectively.

The permeability, porosity, and water content values for backfill cited in Tables 4.1 and 4.2 were estimated in consultation with Rockwell's staff[4].

---

[4] Guidance provided by Rockwell at a meeting held between Rockwell, LBL and KE/PB at Oakland June 2, 1982.

The values given in Table 4.1 for thermal conductivity, specific heat, and density of the backfill are those reported by Anderson (1982). We have estimated the range of values given in Table 4.2 for these parameters. Because the resaturation calculations are very sensitive to the assumed porosity of the backfill, a large range of values is given.

4.3.3 Heat Transfer Coefficient

The heat loss from the entablature rock mass and waste canisters to the storage room consists of two components: convective and conductive heat loss. The numerical simulations accurately account for the convective heat transfer by modelling the fluid flow into the storage room. Calculation of the conductive heat losses is more difficult as it involves heat transfer from the storage room walls to the moist air inside the storage room. A rigorous analysis would require detailed modelling of the air/steam/water flow regime within the storage room. In the present studies, approximate calculations of conductive heat loss were made. An overall heat transfer coefficient, h, which is defined by the expression:

$$Q_h = h\ (T_r - T_{sr}) \quad , \tag{4.3}$$

was used, where h is the heat transfer coefficient, Q is the heat flux per unit area, T_r is the temperature of the rocks adjacent to the storage room, and T_{sr} is the room temperature.

There are not sufficient data at present to compute heat transfer coefficients for the BWIP reference repository design. In a simulation study of a similar system, Eaton and Reda (1981) assumed a value of H = 25 $W/m^{2}{}^{\circ}C$. This value was used for the reference case (Table 4.1), and a range of 10-50 $W/m^{2}{}^{\circ}C$ was selected for the sensitivity calculations (Table 4.2).

4.3.4 Thermal Properties of Air

The thermal properties of the air in the underground openings, cited in Table 4.1, were taken from standard references. No parametric studies involving these parameters were required.

4.3.5 Properties of the Canisters Storage Hole Plug

It was assumed that the plugs located at each end of the canister storage holes will be made of concrete, but designed to permit free passage of fluids flowing out of the hole. Therefore, in the simulation studies, we assigned a large value of permeability to the element representing the plug. The thermal properties for the plug that are cited in Table 4.1 were obtained from standard references. Their influence on the results of the analyses are insignificant and, thus, single values were used throughout the study.

4.4 Canister Heat Generation Rates

In the simulation studies we only consider commercial high level waste (CHLW) and assume that the canisters are emplaced in the repository 10 years after removal of the fuel from the reactor core. The thermal load per canister at the time of emplacement is 2.21 kW (Slate, 1981). The decline in thermal output per canister over time is given in Table 4.3 (Slate, 1981).

Table 4.3. Relative heat-generation rates for ten year old CHLW canisters.

Time after emplacement (yrs)	Relative heat-generation rates
0	1.0
5	0.849
10	0.723
15	0.621
20	0.539
30	0.424
40	0.361
50	0.330
70	0.285
90	0.132
990	0.009
9990	0.0008

5. RESULTS FOR THE REFERENCE CASE

5.1 General Phenomenology

Before quantitative results of the analyses performed for the reference repository design (RRD) are presented, a brief qualitative outline will be given of the thermal and hydrologic processes that will occur in the repository. This will facilitate presentation of the numerical results and clarify the approach used in the simulations.

It is assumed that the waste packages are emplaced "hot"; at a temperature of 300°C. In low permeability rocks, most of the heat generated by the canisters is removed by thermal conduction. After emplacement in a relatively cool (54°C) host rock, canister temperatures initially decline, but, within a few days, heat loss to the rock decreases to a level below the rate of heat generation in the canisters. Subsequently, both temperatures and temperature gradients increase everywhere in the system, with the largest changes increases occuring in the immediate vicinity of the canister storage hole. About two years after emplacement, temperature gradients have increased to the point where all generated heat is being removed from the canisters. This causes canister temperatures to first stabilize, and then to slowly decline as heat output diminishes. At greater distance from the canister storage hole, temperatures remain lower, and maximum temperatures are reached somewhat later.

Prior to backfilling, canister storage holes and storage rooms are close to atmospheric pressure (1 bar), while groundwater pressure at the depth of the reference horizon is approximately 130 bars (13 MPa). This causes pore fluids to migrate toward the pressure sink (canister holes and storage rooms). Due to the small compressibility of liquid water, the pressure pulse

diffuses rapidly outward, away from storage rooms and canister holes and reaches the boundaries of the low-permeability zone in a matter of days. Subsequently, a quasi steady flow field is maintained throughout the open period of the repository, with water influx at the boundary of the low permeability zone closely matching discharge into the excavation. Minor changes in fluid flow occur with variations in fluid mobility, caused by the temperature dependence of viscosity. There are also small effects on fluid flow due to fluid boiling in the rock mass immediately surrounding the openings.

As water flows toward the excavations, temperatures generally increase, while pressures diminish to 1 bar at the walls of the storage rooms and canister holes. In a small region of a few inches around the canister hole, pressures drop below the water vapor pressure for the prevailing temperatures in the rock, causing water to flash into steam. The steam migrates into the canister hole and along the air gap around the canisters into the storage room. Other pore fluid is discharged through the storage room walls in liquid form, and is subsequently partially vaporized in the storage room, with heat of vaporization supplied by conduction.

At the reference formation permeability of $k = 10^{-18}$ m^2 ($\equiv$ 1 microdarcy), total fluid flow into the storage room is approximately 3×10^{-4} kg/s per canister; with minor variations over several decades after emplacement. Approximately 60 % of the total flow is steam expelled from the canister hole; the remainder is liquid water from the storage room walls. For the temperatures of interest here, steam has a specific enthalpy of approximately 2.75 MJ/kg so that steam flow removes heat from the canisters at a rate of approximately 0.5 kW per canister. This is a substantial fraction of canister

output, which is 2.21 kW at t = 0 years, and 1.6 kW after 10 years. The heat removed from the system by liquid water discharging into the room is rather small, typically 75 W per canister. Thus, even at the low permeability of 10^{-18} m^2, steam flow can remove a significant fraction of total generated heat. Steam flow is important only in the void space in the canister hole; steam zones in the host rock are negligible (see below).

5.2 Extent of Steam Zone in the Rock Mass

Because the steam zone in the rock adjacent to the canister hole walls is extremely small, very fine spatial resolution is required in the numerical simulation. Table 3.1 gives the geometric specifications of the "fine mesh" employed in the high resolution calculations. This, together with the model parameters (Table 4.1) and the time-dependent heat generation rates (Table 4.3), defines the numerical simulation problem for the reference case. Results for the volume of rock in which boiling occurs are given in Appendix A (Figure A1). This volume is

$$V_{boiling} = \sum_{S \neq 0} V_n \quad , \tag{5.1}$$

where the sum extends over all volume elements in the model which at a given time contain some steam. The discontinuities in Figure A1 occur because of the finite space discretization. Whenever a volume element makes a phase transition, $V_{boiling}$ "jumps" by a finite amount. Note that all results are presented for the entire system modelled (8.5 canisters), so that the boiling volume per canister is 1/8.5 times the value plotted in Figure A1. The maximum rock volume in which boiling occurs is 0.46 m^3 per canister; this value is reached 10 months after emplacement, at which time boiling extends to a radial distance of 13.2 cm beyond the wall of the canister hole. The

total volume of steam present in the host rock is

$$V_{steam} = \sum_n \phi_n S_n V_n \quad , \tag{6.2}$$

which is plotted as a function of time in Figure A2. Steam volume per canister reaches a maximum of 0.30×10^{-3} m^3 after 1.3 years. This is extremely small in comparison with void volumes per canister of 30.4 m^3 and 0.87 m^3 in the storage room and canister hole, respectively. Therefore, the impact of drying of the rock mass on resaturation times is negligible. Figures A1 and A2 show, furthermore, that the very small rock volume dried at early times is resaturated after 44 years, or before backfilling and decommissioning of the repository.

In the two-phase (steam) zone formed near the canister hole walls, total fluid mobility is smaller than in the pure-liquid case, giving rise to an additional pressure drop across this zone. However, because of the small extent of the two-phase zone, the impact on fluid flow is negligible.

5.3 Fluid Flow, Temperatures, and Pressures

The fine mesh calculations described above are costly because of the very small volume elements near the canister hole wall and the associated limitations in computer "throughput" and the small time steps required. Calculations with a coarse mesh, with dimensions as specified in Table 4.2, are much more efficient. In Figures A3 through A14, both fine and coarse mesh results are presented for pressures and temperatures as a function of radial distance from the canister hole center line. The results are given for the fourth layer of elements (z = 10.1 m) from the storage room center plane, at times of approximately 1.5 months, 1 year, and 20 years. In all cases results for the fine and coarse mesh agree to within line thickness,

thereby demonstrating that the coarse mesh is adequate for predicting pressures and temperatures. There is only one substantive difference between the results produced by the two models: temperatures and pressures in the coarse mesh are averaged over a larger region around the canister hole, so that no boiling occurs in the rock. Therefore, the coarse mesh is adequate for all aspects of the problem, except for predicting the extent of the steam zone in the rock. However, the results from the fine mesh calculations, show that the extent of this zone is negligible.

Additional results for the reference case are given in Figures A15 through A24. These are all based on "coarse mesh" calculations. Figures A15 and A16 show that at all times total fluid flow into the storage room is essentially equal to total fluid flow at the boundary of the model. This demonstrates that quasi-steady flow conditions are present at all times due to the low fluid compressibility. The changes in the total flow with time illustrated in Figures A15 and A16 are caused by the dependence of the fluid viscosity on temperature. At early time the mass flux increases due to heating of the rocks surrounding the canister hole. Later, as the thermal output from the canisters decreases, the temperatures in the rock decrease and the flow rate diminishes. This effect can also be seen in Figures A17 through A19, which show radial pressure profiles (for the layer of elements at z = 10.1 m) at three different times. The figures show that the profiles are only weakly time-dependent. The curvature seen in Figures A17 through A19 is caused by the temperature dependence of viscosity that causes smaller pressure gradients near the canister hole wall for a given mass flux than near the outer boundary. If the fluid mobility were constant, the curve on a plot of pressure versus the logarithm of radial distance would be linear.

Figures A20 and A21 show the time-dependence of pressure and temperature at selected elements in the layer corresponding to z = 10.1 m. The highest temperatures occur at this distance from the storage room center plane due to an interplay of convective heat flow into the canister hole and conductive heat transport into the rock. The highest canister element temperature predicted is 210°C, which is reached approximately 2 years after emplacement. One must bear in mind that the canister element peak temperatures may differ somewhat from the peak temperature of the canisters themselves because we do not model heat transfer in the air gap between the canisters and the canister hole walls in detail (see Sections 3.4 and 8.0). The highest average rock temperature in the region 0.343 m $\leq$ r $\leq$ 0.995 m around the canister hole is 165°C. The fine mesh calculation gives a maximum average rock temperature in the region 0.343 m $\leq$ r $\leq$ 0.387 m of 191.9°C, with a maximum canister element temperature of 208.6°C.

Figures 22 through 24 give radial temperature profiles in the rocks at z = 10.1 m, for various times after canister emplacement. At late time (7407.41 days, or 20.3 years) the temperature gradient is linear on a logarithmic scale of radial distance, indicating a steady conductive heat flux radially outward from the canister hole. The kinks in the curve that occur at r = 0.7 m and r = 15 m, are due to the effects of the canister hole and the outer boundary of the model, respectively. Comparison of these results with temperature profiles at earlier times shows how the region of steady heat flux is gradually expanding outward with time. For the model parameters used, the thermal diffusivity is orders of magnitude smaller than hydraulic diffusivity, so that the zone of quasi-steady heat flow expands much less rapidly than the zone of quasi-steady fluid flow.

5.4 Resaturation Time

To complete the discussion of the reference case we will now consider the resaturation process. It is assumed that storage rooms and canister holes are backfilled 50 years after canister emplacement. Backfill temperature is assumed to be 27 °C, and other backfill parameters are given in Table 4.1. Because several critical backfill parameters, such as porosity and water content, will depend on the design of the materials and placement techniques, they cannot be precisely specified at the present time. Therefore, it was assumed that the properties of backfill in storage rooms and canister holes were identical. To investigate the dependence of saturation time on backfill properties, calculations were made for a full range of void ratios (0-1000%).

The resaturation calculations were started with rock mass temperatures and pressures as computed for 50 years after canister emplacement, but temperatures in the storage room and in the backfilled space around the canisters were assumed to be 27 °C. The void space in the backfill, which will be air-filled when the material is placed, was represesnted as steam-filled in the model. This approximation is similar to that made for the initially air-filled spaces in the storage rooms and canister holes, and is satisfactory for the purposes of the analyses. In the resaturation calculations we do not consider spatial dependence of pressure in the backfill in storage rooms and canister holes. This approximation will lead to somewhat lower resaturation times, but it appears conservative and adequate for the present studies. Resaturation was computed for backfill porosities of ϕ = 5%, 50%, and 100%; the last value corresponding to the limiting case

where no backfilling is used, yielding an upper limit for resaturation time. Figure 5.1 shows that the resaturation time depends linearly on porosity, which was to be expected because the void volume to be resaturated is proportional to porosity. For the reference case with a porosity of ϕ = 25%, the resaturation time, t_{res}, is predicted to be 1.6 years.

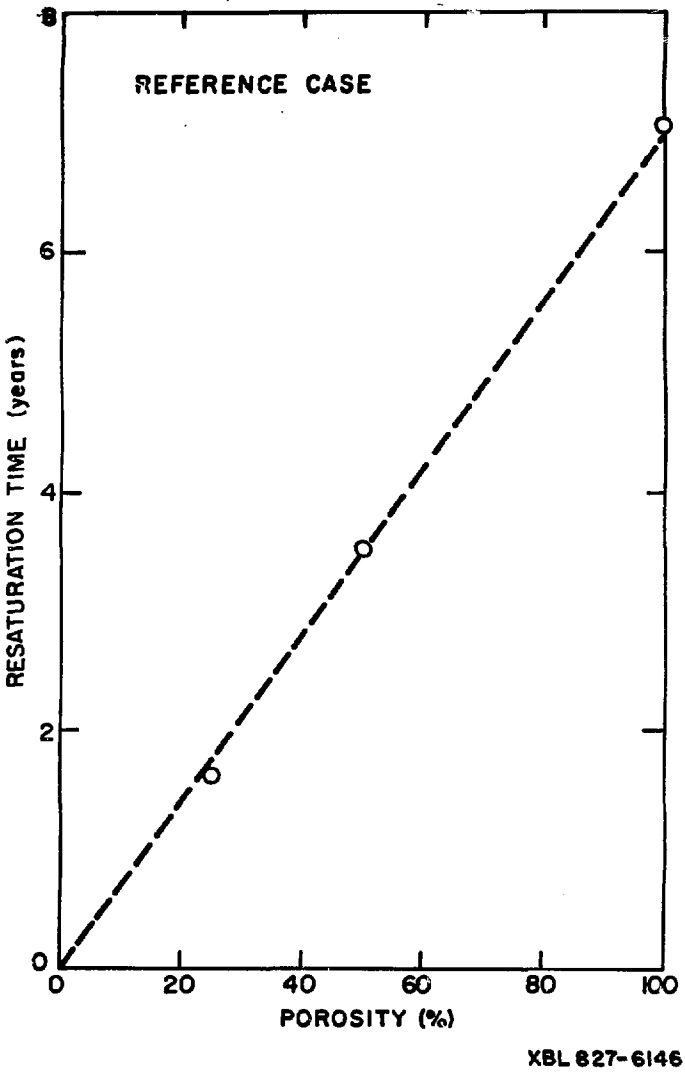

FIGURE 5.1 Resaturation time versus porosity of backfill.

6.0 RESULTS OF SENSITIVITY STUDIES

In Section 4 we noted that some of the important site-specific parameters are not well known at the present time. It is therefore helpful to determine the sensitivity of our predictions to uncertainties in such key parameters as formation permeability, backfill porosity, thermal conductivity, and boundary conditions. In some cases it was advantageous to study limiting cases where some parameters were given extreme (and unrealistic) values because this can help to clarify the effects of different physical processes. For example, if permeability is very small, advective heat transport will be negligible. The resulting temperature profiles correspond to a "pure conduction" case. Comparison with (more realistic) higher, permeability cases then made it possible to assess the impact of advective heat transport upon predicted temperatures. In the sensitivity studies we use the range of values given in Table 4.2 as guidelines.

The sensitivity studies performed are summarized in Table 6.1. Except for the parameters noted in the table, each case employed the input values used for the reference case. These studies are not not intended to be exhaustive; rather, the purpose was to vary parameters which are not accurately known but which may have a significant impact on the thermohydrological performance of the repository. The studies show that most parameters influence repository performance in rather simple ways, so that a limited number of cases is sufficient to illuminate expected trends.

The following discussion will compare the various cases with the reference case (Section 5). Our presentation will selectively focus on differences and similarities and stress the most important issues: evolution of

Table 6.1: Sensitivity Studies

Case	Modified Parameter(s)	Reference Value	Modified Value	Units	Description
1	Permeability	10^{-18}	10^{-20}	m^2	Very Low Permeability
2	Permeability	10^{-18}	10^{-17}	m^2	Large Permeability
3	Porosity	0.1	1	%	Large Porosity
4	Heat conductivity	2.30	1.15	W/m°C	Small Heat Conductivity
5	Boundary pressure	130	65	bars	Small Boundary Pressure
6	Boundary pressure	130	30	bars	Very Small Boundary Pressure
7	Heat transfer coefficient	25	50	$W/m^2°C$	Large Heat Transfer Coefficient
8	Heat transfer coefficient	25	10	$W/m^2°C$	Small Heat Transfer Coefficient
9	Permeability Heat conductivity Boundary pressure	10^{-18} 2.30 130	10^{-20} 1.15 30	m^2 W/m °C bars	Extreme Case

temperatures with time, evolution of steam zones (if any), rate of fluid flow into the storage room, and resaturation time after backfilling.

6.1 Case #1 - Very Low Permeability

It was noted in Section 5 that heat conduction is the dominant cooling mechanism in the reference case, but advective heat transport makes a significant contribution by removing approximately 25% of canister output. To assess the impact of advective heat flow in more detail, a case with an extremely low rock permeability (10^{-20} m^2) was studied. It is two orders of magnitude lower than the reference permeability. We do not suggest that the BWIP reference horizon will have such an extraordinarily low permeability; rather, we present an extreme case to illustrate the effects of negligible advective heat flow. Figures B1 through B4 (Appendix B) show some results for this case.

Total fluid flow into the storage room is closely equal to 1% of that calculated for the reference case (Figure B1), but is actually approximately 5% larger than would be predicted from simple proportionality to permeability. This is due to the somewhat higher temperatures throughout the system (Figure B4) resulting in slightly lower viscosities. The pressure response at the boundary is delayed significantly by the low permeability, so that fluid flow from the boundary increases more slowly and peaks at a later time than flow into the room (Figures B1 and B2).

The pressure transients in the rock are very similar to those in the the reference case (Figure B3), but temperatures increase more rapidly and reach higher values (Figure B4). The predicted peak canister element temperature is 230°C, which is about 20°C higher than that in the reference case.

Therefore, the steam zone is expected to be slightly larger, but the model shows no steam present in the rock because in the "coarse mesh" calculations, the radial elements adjacent to the canister storage hole are larger than the zone in which boiling occurs.

6.2 Case #2 - Large Permeability

In this case we use a tenfold larger value of the rock permeability than was employed in the reference case. The value used in these calculations, $k = 10^{-17}$ m^2, is potentially realistic for the Umtanum entablature rocks (King et al. 1981). Total fluid flow into the storage room is approximately ten times that for the reference case (Figure B5). The increase is slightly less than tenfold because temperatures are lower and fluid viscosities higher (Figure B5). Within computational accuracy, fluid flow into the storage room is equal to recharge from the boundary at all times (Figure B6). Pressure transients are again similar to those in the reference case (Figure B7), but temperatures remain much lower, never exceeding 100°C anywhere in the system (Figure B8). Considering that in the reference case approximately 25% of canister heat output was removed by advective transport, it was to be expected that a tenfold increase in fluid flow rates would remove essentially all generated heat by advection. Canister element temperatures rise to 100°C, because this temperature is needed to vaporize the incoming water at the prevailing atmospheric pressure. Fluid flow rates are not sufficient to remove all generated heat by liquid water with its much smaller heat content. At 100°C, $h_{liquid} = 419.0$ kJ/kg, so that at the computed flow rate of approximately 2.47×10^{-3} kg/s per canister, liquid water can remove heat at a rate of only 1.03 kW per canister, or approximately 50% of canister output. Therefore, permeabilities greater than 2×10^{-17} m^2 would be

needed to remove all heat by advection without boiling in the canister hole.

6.3 Case #3 - Large Porosity

The porosity of the Umtanum Entablature is not well known. Variations in porosity have three effects: (1) changing the time scale (diffusivity) for the propogation of pressure disturbances, (2) modifying the volumetric specific heat of the rock-water mixture, and (3) changing the steam volume within a rock mass of given size. As discussed previously, pressure transients are rapid, volumetric specific heat is dominated by the rock, and boiling is confined to a very small volume of the rock mass. Therefore, porosity variations are not expected to have significant impact upon repository performance.

Simulations assuming a tenfold increase in porosity (ϕ = 1.0%, as compared to the reference case, ϕ = 0.1%) confirm the above evaluation. Results for fluid flow, pressures, and temperatures (Figures B9 through B12) all agree to within line thickness with those obtained for the reference case. Therefore, porosity effects will be negligible as long as porosity does not exceed a few percent.

6.4 Case #4 - Small Heat Conductivity

The references cited in Section 4 suggest that the heat conductivity of the host rock may be substantially smaller than the value of 2.30 W/m°C used for the reference case. Several studies indicate values close to 1.15 W/m°C, which is the value adopted for Case #4 of the sensitivity studies. Figures B13 through B17 show that heat conductivity has a very strong impact

on repository performance. When K is assumed to be 1.5 W/m°C, the peak canister element temperature is 365°C, which is 155°C higher than that in the reference case (Figure B15). A rather peculiar fluid pressure behavior is predicted (Figure B16), caused by the development of an extended boiling zone (Figure B17). A maximum steam volume in the host rock of 6.7×10^{-3} m^3 per canister is reached after 4.1 years. Steam is much less mobile than liquid water, so that pressures near the canister storage hole rise to relatively large values. Nonetheless, the mass flow into the storage room remains below that for the reference case for seven years, due to lower fluid mobilities (Figure B13). As steam volume diminishes (Figure B17), pressures decline while fluid flow continues to rise for some 15 years after emplacement. The steam zone is completely resturated after 20 years. Due to the high temperatures near the canister storage hole, mass flows remain somewhat higher than those in the reference case.

6.5 Cases #5 and #6 - Small Boundary Pressure and Very Small Boundary Pressure

The fluid-carrying capacity of the permeable strata above and below the Umtanum Entablature is not well known at present. It is conceivable that drainage into the excavations over a large repository area for an extended period could cause a significant regional pressure depression. To investigate these possible effects, two studies were made with lower pressures at the outer boundaries (overlying and underlying permeable zones). In Cases #5 and #6 the pressure at the outer boundary was assumed to be 65 bars (6.5 MPa) and 30 bars (3.0 MPa), respectively. In the reference case a value of 130 bars (13.0 MPa) was used, which is the undisturbed pressure at the depth of the Umtanum entablature.

Comparison of figures A15, B18 and B23 shows that the total fluid flow into the storage room is approximately proportional to the boundary pressure. For the case P_{bound} = 30 bars, the flow is actually somewhat lower than expected from simple proportionality because a larger steam zone develops with reduced mobility (Figure B27). Maximum steam volume is 5.4×10^{-3} m^3 per canister for P_{bound} = 30 bars, and 1.3×10^{-3} m^3 per canister for P_{bound} = 65 bars. Thus, the extent of the steam zone is predicted to be negligible even if the boundary pressures is as low as 30 bars. In the case with P_{bound} = 30 bars, complete resaturation occurs within 20 years after emplacement. Due to diminished mass flows there is less convective cooling than in the reference case, giving rise to somewhat higher temperatures. Peak canister element temperatures are 224°C for Case #5 and 230°C for Case #6, (Figures B21 and B26) as compared to 210°C for the reference case.

6.6 Cases #7 and #8 -Large and Small Values of Heat Transfer Coefficient

The heat transfer coefficient describes heat transfer to the storage room by means of buoyancy-driven air flow along the room walls. For the reference case, a value of h = 25 $W/m^2°C$ was used as given by Eaton and Reda (1981), but the actual value will depend on various parameters such as roughness of storage room walls, shape of storage room, air moisture content, small components of forced convection, and other conditions. The effects of this heat transfer mechanism are expected to be small as most of the heat conducted away from the canisters dissipates outward into the rock mass and away from the underground openings rather than being conducted towards the storage room walls. Simulations with h = 50 $W/m^2°C$ (Case #7) and 10 $W/m^2°C$ (Case #8) were carried out, with results shown in Figures B28

through B35. The results for the two cases are virtually indistinguishable, with the case of lower heat transfer coefficient yielding slightly higher temperatures ($\leq$ 1°C).

6.7 Case #9 - Extreme Case

In order to place an upper limit on the volume of rock within which boiling occurs, several extreme parameter choices were combined to yield a greater extension of the steam zone. Permeability was reduced by a factor of 100 from the reference value to suppress convective cooling (See also Case #1). At the same time, heat conductivity was assumed as 1.15 W/m°C, as in Case #4. These two parameter values yield the highest temperatures in the vicinity of the canisters. To further increase the volume of the steam zone, boundary pressure was reduced to 30 bars (3MPa, see Case #6).

Results obtained from a "fine mesh" calculation (see Section 3.0) are given in Figures B36 through B41. At early times fluid flow into the storage room declines because of the evolution of a steam zone around the canister hole. As the boiling zone migrates outward, fluid mobility generally diminishes, consequently reducing pore pressures (Figure B38) and flow rates (Figure B36). Superimposed on this general decline are several effects which produce a non-monotonic pressure- and flow rate-response: (1) temperatures increase for a period (Figure B39), enhancing fluid mobility in the outer (single-phase liquid) region; (2) as liquid saturations decline in the boiling zone, total mobility of the two-phase fluid diminishes at first and then increases somewhat as steam saturation approaches 1.0 (this effect is due to changes in relative permeabilities); (3) the finite space discretization used in the simulation causes the steam front to propagate in "jumps",

as successive radial elements start to boil. This is evident in Figure B40, which shows the boiling rock volume as a function of time. Maximum dried rock volume per canister is 30.0 m^3, and the maximum steam volume per canister is 29.6 x 10^{-3} m^3. This volume of steam, though larger than in all of the other cases, is still negligible compared to the void volumes in the canister storage hole and storage room. The maximum radial extent of the boiling zone is 1.36 m beyond the wall of the canister hole. Resaturation of the dried rock volume begins 19 years after emplacement (Figure B41), and is almost complete at the time of backfilling (50 years).

The maximum temperature in the second canister element away from the wall of the storage tunnel (z = 10.1 m) is 366°C, only slightly higher than in Case #4. Due to the combined effects of conduction and convection, this was the canister element with the highest temperature in Case #4, whereas, in this case the highest temperatures were observed at maximum distance from the tunnel wall. At z = 31.0 m, a maximum temperature of 385.8°C occurs after 4.4 years. Maximum rock temperature at this time is 353.8°C.

6.8 Resaturation

The time required for resaturating the storage tunnel room and canister storage hole after they have been backfilled depends upon the porosity of the backfill, and the rate of fluid flow into them. Porosity dependence in the reference case was discussed in Section 5. In this section the dependence of resaturation time on fluid flow is considered.

Fluid flow rates are only weakly dependent on all parameters except permeability and boundary pressure. It was noted previously that fluid flow rates are proportional to boundary pressures, except for minor corrections

from thermal and two-phase effects. Therefore, to a good approximation, resaturation times are inversely proportional to boundary pressures. A similar relationship holds for permeability. In the absence of thermal or two-phase effects, fluid flow rates would be strictly proportional to permeability. Therefore, resaturation times are approximately inversely proportional to permeability. That is:

$$t_{res} = \text{const}/k \ , \tag{6.1}$$

or

$$\log t_{res} = \log (\text{const}) - \log k \tag{6.2}$$

Resaturation calculations were carried out with a backfill porosity of 25%, for three different values of permeability: 10^{-17} m^2 (Case #2), 10^{-18} m^2 (Reference Case), and 10^{-20} m^2 (Case #1). The results are given in Table 6.2 and Figure 6.1.

If thermal and two-phase effects had no influence, resaturation time would plot as a straight line of slope -1.0 against permeability on log-log paper. Figure 6.1 shows that this is a reasonable approximation. For cases of large permeabilities, resaturation takes progressively longer than expected from simple proportionality because contributions from convective cooling increase fluid viscosity, thereby diminishing mobility. These effects are small, however, so that the linear relationship plotted in Figure 6.1 is sufficiently accurate to permit interpolation of resaturation times for other permeabilities of interest.

Table 6.2: Resaturation times

Permeability (m^2)	Resaturation Time (years)
10^{-17}	0.194
10^{-18}	1.64
10^{-20}	136.4

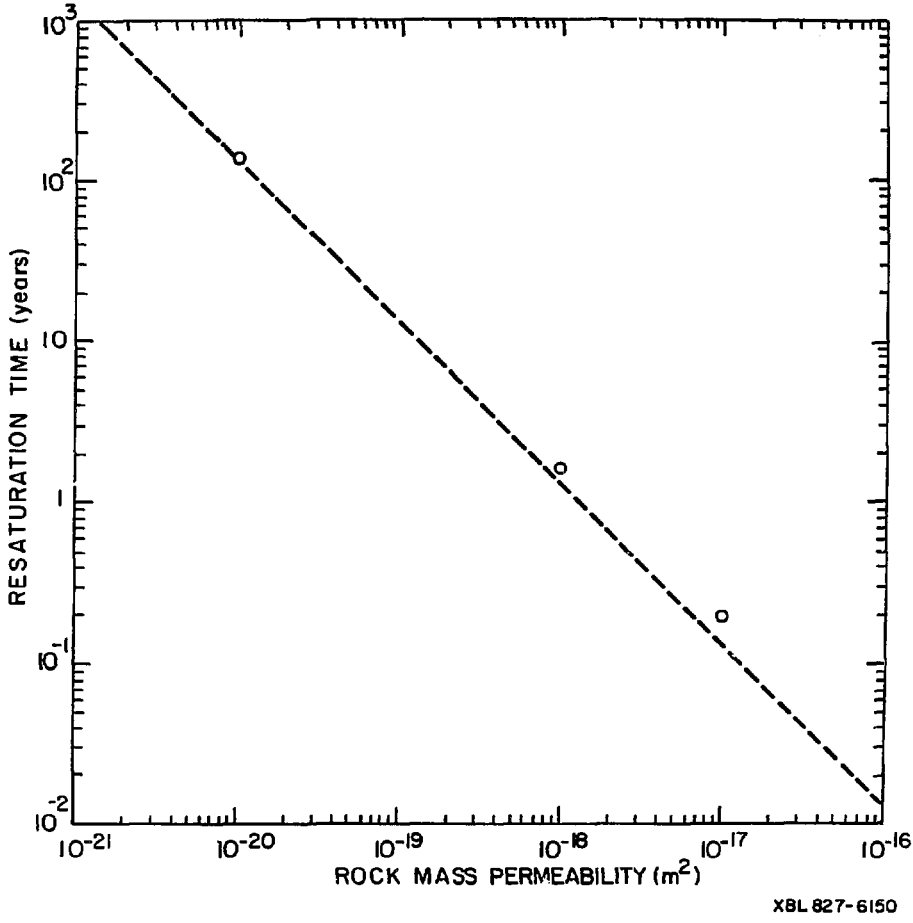

FIGURE 6.1 Resaturation time as a function of rock mass permeability.

7.0 CONCLUSIONS

We have considered room-scale models to numerically simulate thermohydrological conditions in a high-level nuclear waste repository constructed in Pasco basin basalts. Approximations used in the analyses include a two-dimensional representation of storage room and canister hole geometry, and a porous medium treatment for the rock mass, which in actuality is fractured and has a low matrix permeability. These approximations are believed to have little impact upon the principal results which are summarized below.

(1) Even for rather extreme assumptions for site-specific parameters, the predicted volume of rock dried by steam formation is negligible compared to the excavated voids in storage tunnels and canister holes. Except under extreme and unlikely conditions, the host rock will completely resaturate before the end of the 50-year open period and prior to backfilling.

(2) Advective heat transport is an important cooling mechanism, contributing approximately 25% of the canister heat loss if the rock mass permeability is 10^{-18} m^2, and dominating over conductive heat loss if the permeability is 10^{-17} m^2 or larger.

(3) Fluid flow into the storage room is approximately proportional to rock mass permeability, with a typical value of 2.9×10^{-4} kg/s per canister for a rock mass permeability of 10^{-18} m^2.

(4) Canister temperatures are very sensitive to the thermal conductivity of the rock, and also to rock mass permeability if the latter exceeds 10^{-18} m^2.

(5) Resaturation times after backfilling will strongly depend upon host rock permeability but, within reasonable limits, only slightly upon other parameters. For the most probable parameter values resaturation time is predicted to be less than two years.

8.0 RECOMMENDATIONS FOR FUTURE STUDY

The present study was limited in scope to a room-scale approach, and employed a number of idealizations and approximations commensurate with existing knowledge about the site and available modeling capabilities. This section identifies issues which warrant further study to improve the reliability of predictions for the thermohydrological performance of a high-level waste repository in basalt.

8.1 Flow Geometry

The present study employed a two-dimensional axisymmetric model, whereas the actual repository system is three-dimensional. The important system features were preserved and the error introduced by these approximations are not expected to influence the general conclusions developed from the study. However, it is not possible to formally quantify the accuracy of the 2-D model without comparing the results to a fully three-dimensional calculation. Three-dimensional models require a rather large computational effort, but, to validate the 2-D approach, it would be sufficient to study a small number of representative cases.

8.2 Fractured Porous Medium

The rock mass was approximated as a porous medium. However, the Hanford basalts are fractured and the fractures control fluid flow. Thermodynamic conditions within the fractures may deviate significantly from volumetric averages for larger rock volumes which were considered in the present study. For instance, pore pressures in the fracture system may be lower than in the rock matrix, so that boiling in the fracture system may occur throughout a more extensive volume. Due to the small volume of the fractures this

is unlikely to significantly affect total steam volume in the host rock. However, because steam mobility is much lower than that of liquid water, extensive boiling in the fracture system may reduce fluid flow towards the canister holes, thereby reducing convective cooling. Modeling of these effects is possible by the "multiple interacting continua" method (Pruess and Narasimhan, 1982).

8.3 Regional Hydrology

Regional groundwater flow may significantly affect thermohydrologic conditions in the near field of storage rooms. If the higher permeability strata above and below the Umtanum cannot readily replenish the fluid being discharged into the repository excavations, the pore pressures at the Umtanum boundaries will decline with time. This possibility was addressed in sensitivity studies on boundary pressures. For a more realistic assessment, models should be developed to quantitatively represent the interaction between the repository as a whole and the surrounding geological and hydrological units. These interactions could have important effects upon thermohydrologic conditions in the near field of storage rooms. The dried rock volume could become large if boundary pressures decline sufficiently.

8.4 Canister Temperatures

It was assumed that temperatures inside the canister storage hole are uniform over the distance between the canister axis and storage hole wall. No attempt was made to model the detailed physical processes (radiation, fluid or gas convection, and conduction) which control heat transfer from the canister to the surrounding rock. The simplification used for the

for the present analysis are adequate for modeling temperatures within the rock, because the heat discharged into the rock must always be closely equal to the difference between heat generated by the canisters, and heat lost to fluid convecting past the canisters into the storage room. Canister temperatures, however, are controlled by the small deviations from quasi-steady heat flux conditions, which depend upon the detailed heat transfer mechanisms in the void spaces in the canister storage hole. These processes must be modeled if a more accurate prediction of canister temperatures is desired.

8.5 Schedule of Repository Development and Operation

Repository development and waste loading will extend over a long period. The excavations will take years to complete, and waste emplacement schedules will extend over decades. The duration and sequence of repository operations may significantly impact upon repository performance, and these effects should be quantified.

8.6 Resaturation

In the resaturation calculations we did not consider spatial variations in pressure within the storage tunnel and canister hole backfill. This approximation is expected to somewhat underestimate resaturation times. Constant values for backfill permeability and porosity were also assumed. The resaturation process will cause the clay components of the backfill to swell, so that material properties may become a function of time and space. These effects may have a significant influence on the time required for resaturation (probably tending to lengthen it) and should be investigated when the backfill material properties are sufficiently defined.

Acknowledgements

The authors would like to thank LBL staff for their help in developing this study, and in the preparation of the manuscript. In particular, the valuable assistance in the numerical analyses provided by Peter Fuller is gratefully acknowledged.

REFERENCES

Agapito, J.F.T., Hardy, M.P., and St. Laurent, D.R., 1977, Geo-Engineering Review and Proposed Program Outline for the Structural Design of a Radioactive Waste Repository in Columbia Plateau Basalts. RHO-ST-6, Rockwell Hanford Operations, Richland, Washington

Anderson, W.J., 1982, Conceptual Design Requirements for Spent Fuel, High Level Wastes and Transuranic Wastes Package Rockwell International, Rockwell Hanford Operations SD-BWI-CR-005 75 p.

Apps, J.; Doe, T; Doty, B.; Doty, S.; Galbraith, R.; Kearns, A.; Kohrt, B.; Long, J.; Monroe, A.; Narasimhan, T.N.; Nelson, P.; Wilson, C.R.; Witherspoon, P.A., 1979, Geohydrological Studies for Nuclear Waste Isolation at the Hanford Reservation, Vol. II, Final Report LBL 8764 (H-94) 260 p.

Colorado School of Mines, 1979, Determination of Basalt Physical and Thermal Properties at Varying Temperatures, Pressures, and Moisture Contents, Second Progress Report, Fiscal Year 1979, RHO-BWI-C-54 Rockwell Hanford Operations, Richland, Washington

Colorado School of Mines, 1979, Determination of Basalt Physical and Thermal Properties at Varying Temperatures, Pressures, and Moisture Contents, Third Progress Report, Fiscal Year 1979, RHO-BWI-C-55 Rockwell Hanford Operations, Richland, Washington

Colorado School of Mines, 197[illegible], Excavation Engineering and Earth Mechanics Institute Final Report for Fiscal Year 1978 on the Physical and Thermal Properties of Basalt Cores, RHO-BWI-C-38 Rockwell Hanford Operations, Richland, Washington

Deju, R.A. and Fecht, K.R., 1979, Preliminary Description of Hydrologic Characteristics and Contaminant Transport Potential of Rocks in the Pasco Basin, South-Central Washington, RHO-BWI-LD-20, Rockwell Hanford Operations, Richland, Washington

Duff, I.S., 1977, MA28 - a set of FORTRAN subroutines for sparse unsymmetric linear equations, AERE Harwell report R8730.

Eaton, R.R. and Reda, D.C.,1981, The influence of Convective Energy Transfer on Calculated Temperature Distribution in Proposed Hard-Rock Nuclear Waste Repositories, paper AIAA-81-1084, presented at AIAA 16th Thermophysics Conference, Palo Alto, California, June 1981

Erikson, R.L. and Krupka, K.M., 1980, Thermal Property Measurements of Pomona Member Basalt from Core Holes DB-5 and DB-15, Hanford Site, Southeastern Washington RHO-BWI-C-76 (H-8) 34 p.

Foundation Sciences, Inc., 1981, Thermal/Mechanical Properties of Umtanum Basalt Borehole DC-2 RHO-BWI-C-92 (H-145) 115 p.

Foundation Sciences, Inc., 1980, Thermal/Mechanical Properties of Pomona and Umtanum Basalts-Elevated Temperature Comparative Triaxial Test RHO-BWI-C-91 (H-146) 75 p.

Foundation Sciences, Inc., 1980, Thermal/Mechanical Properties of Pomona Member Basalt, Full-Scale Heater Test #1 RHO-BWI-C-77 Rockwell Hanford Operations, Richland, Washington

Gephart, R.E.; Arnett, R.C.; Baca, R.G.; Leonhart, L.S.; Spane, F.A. Jr., 1979, Hydrologic Studies Within the Columbia Plateau, Washington: An Integration of Current Knowledge RHO-BWI-ST-5 500 p. with extensive maps (2 folders)

Gephart, R.E.; Eddy, P.A.; Deju, R.A., 1979, Geophysical Logging and Hydrologic Testing of Deep Basalt Flows in the Rattlesnake Hills Well Number One RHO-BWI-ST-1 133 p.

International Formulation Committee,1967, A Formulation of the Thermodynamic Properties of Ordinary Water Substance IFC Secretariat, Dusseldorf, Germany.

Isherwood, D., 1980, Geoscience data base handbook for modeling a nuclear waste repository, Lawrence Berkeley Laboratory Report UCRL-52719, Vol. 2.

Kaiser Engineers, Inc. & Parsons, Brinckerhoff, Quade and Douglas, Inc., 1980, Nuclear Waste Repository in Basalt, Project B-301 RHO-BWI-CD-38 rev. 3 (H-157) 130 p.

Kaiser Engineers, Inc. & Parsons, Brinckerhoff, Quade and Douglas, Inc., 1982, Nuclear Waste Repository in Basalt, Project B-301, Functional Design Criteria RHO-BWI-CD-38 rev. 4 89 p.

King, I.P.; McLaughlin, D.B.; Norton, W.R.; Baca, R.G.; Arnett, R.C., 1981, Parametric and Sensitivity Analysis of Waste Isolation in a Basalt Medium RHO-BWI-C-94 166 p.

LaSala, A.M. Jr.and Doty, G.C., 1971, Preliminary Evaluation of Hydrologic Factors Related to Radioactive Waste Storage in Basaltic Rocks at the Hanford Reservation, Washington USGS-OFR 68 p.

Martinez-Baez, L.F. and Amick, C.H., 1978, Thermal Properties of Gable Mountain Basalt Cores, Hanford Nuclear Reservation LBL-7038 7 p.

Miller, R.J. and Bishop, R.C., 1979, Determination of Basalt Physical and Thermal Properties at Varying Temperatures, Pressures, and Moisture Contents, RHO-BWI-C-50 Rockwell Hanford Operations, Richland, Washington

Myers, C.W.and Price, S.M., editors, 1981, Subsurface Geology of the Cold Creek Syncline RHO-BWI-ST-14 340 p.

Pruess, K. and Narasimhan, T.N., 1982, A Practical Method for Modeling Fluid and Heat Flow in Fractured Porous Media, Proceedings Sixth SPE-Symposium on Reservoir Simulation (paper SPE-10509), New Orleans, LA, January

Pruess, K., and Schroeder, R.C., 1980, SHAFT 79 User's Manual, LBL-10861, Lawrence Berkeley Laboratory, Berkeley, California 94720

Raymond, J.R.and Tillson, D.D., 1968, Evaluation of a Thick Basalt Sequence in South Central Washington - Geophysical and Hydrological Exploration of the Rattlesnake Hills Deep Stratigraphic Test Well BNWL-776 (H-100) 130 p.

SAI, 1978, Science Applications, Inc., Hydrologic Testing in Borehole DC-2, RHO-BWI-C-36, Rockwell Hanford Operations, Richland, Washington

Slate, S.C., et al., 1981, Reference Commercial High-Level Waste Glass and Canister Definition, PNL-3838, Pacific Northwest Laboratories, Richland, Washington

Stanford Geothermal Program (ed.) Proceedings Special Panel on Geothermal Model Intercomparison Study Sixth Workshop on Geothermal Reservoir Engineering, Stanford University, December 1980

Summers, W.K. and Associates, 1973, Descriptions of Wells Penetrating the Wanapum Basalt Formation in the Pasco Basin Area, Washington RHO-BWI-C-22 185 p. with maps

APPENDIX A

COMPUTER GENERATED PLOTS OF RESULTS FOR THE REFERENCE CASE

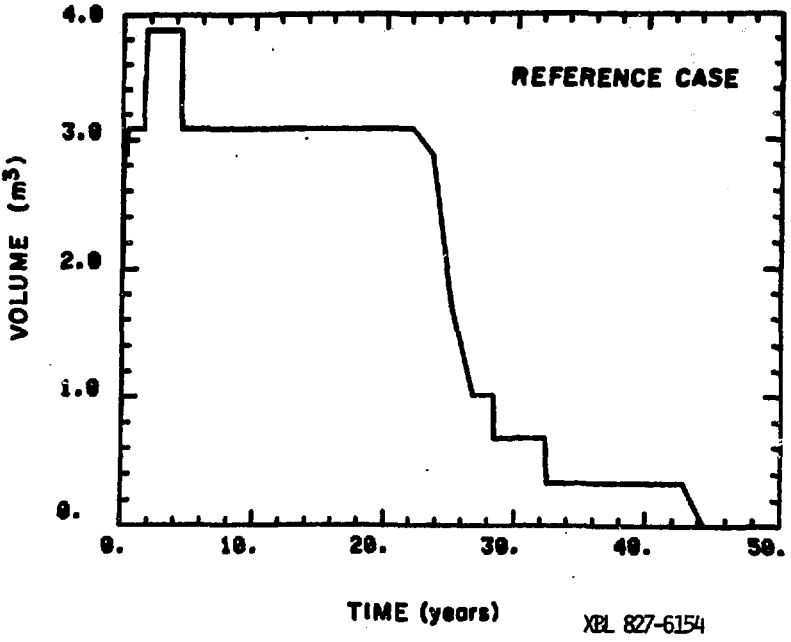

FIGURE A.1 Volume of rock in which boiling occurs (reference case - fine mesh).

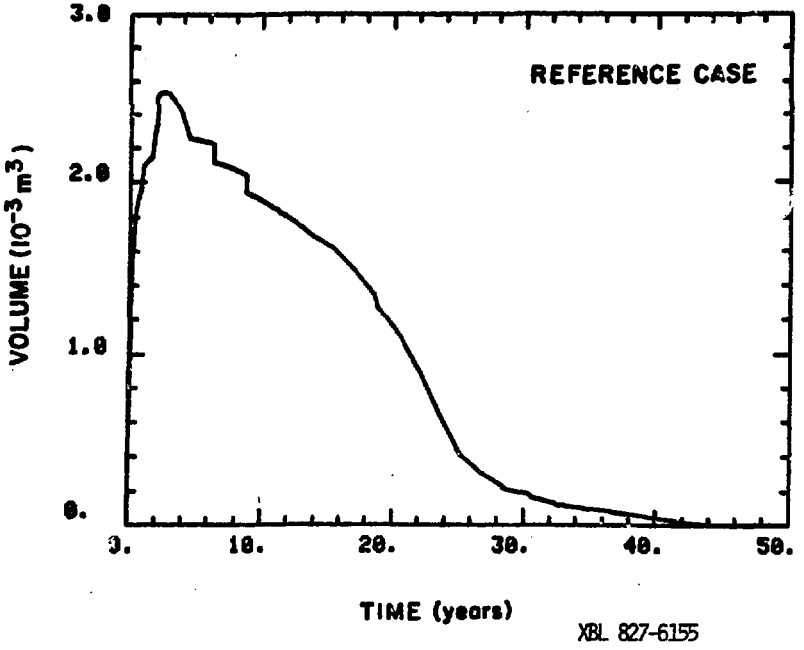

FIGURE A.2 Volume of steam in rock mass (reference case - fine mesh).

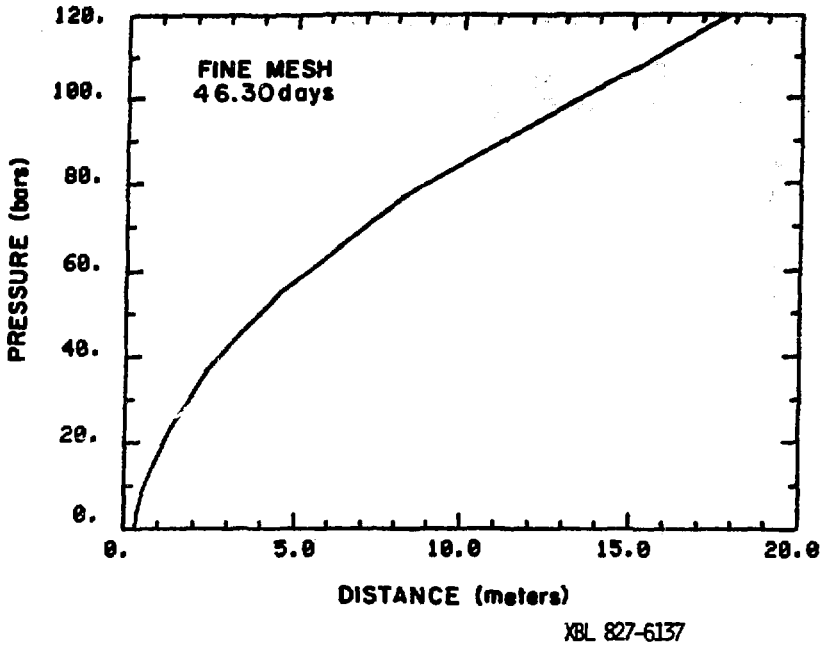

FIGURE A.3 Pressure vs. distance from centerline of canisters after 1.5 months - reference case fine mesh (z = 10.1 m).

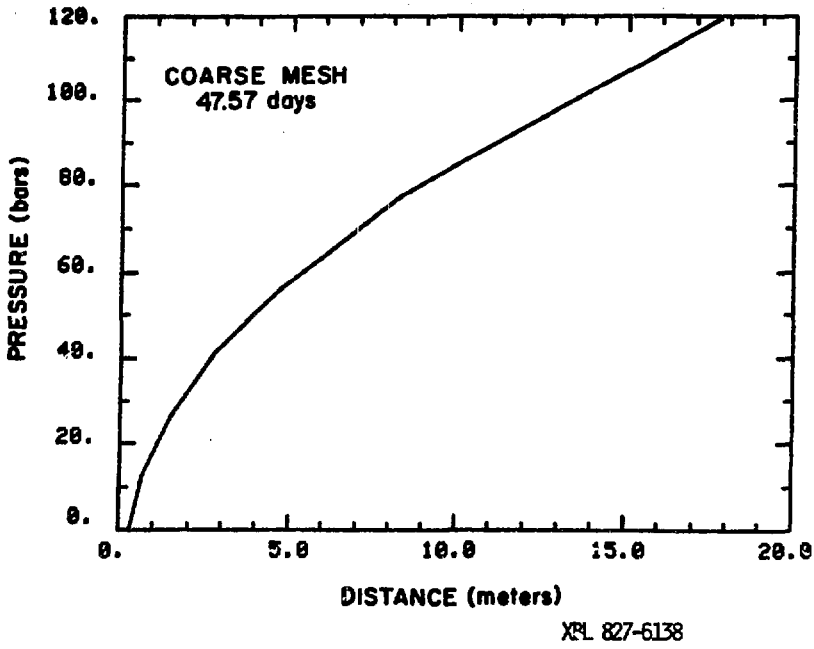

FIGURE A.4 Pressure vs. distance from center line of canisters after 1.5 months - reference case coarse mesh (z = 10.1 m).

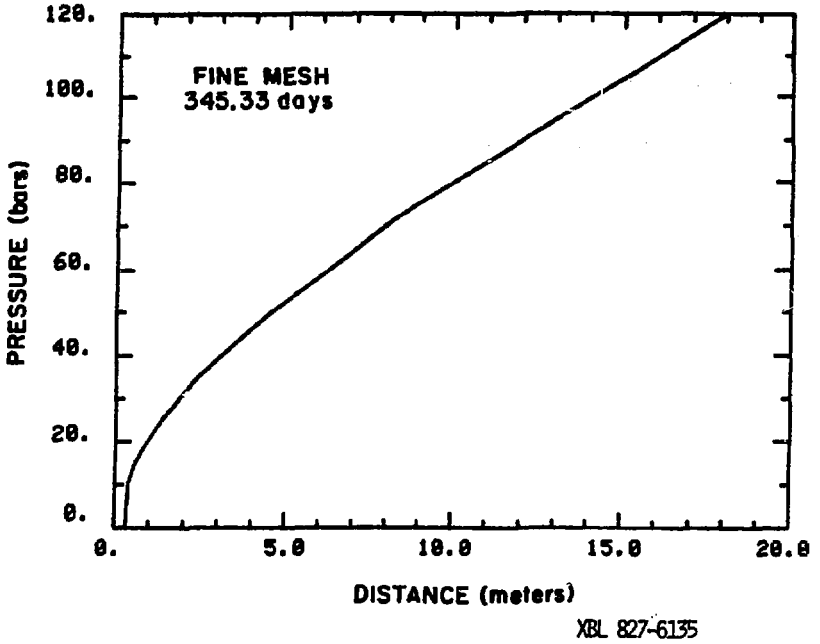

FIGURE A.5 Pressure vs. distance from centerline of canisters after 1 year - reference case fine mesh (z = 10.1 m).

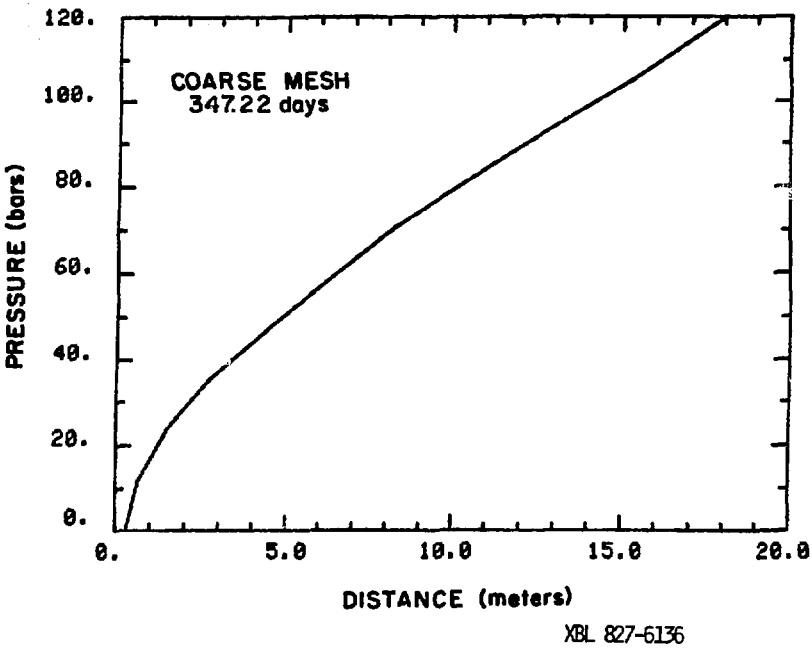

FIGURE A.6 Pressure vs. distance from center line of canisters after 1 year - reference case coarse mesh (z = 10.1 m).

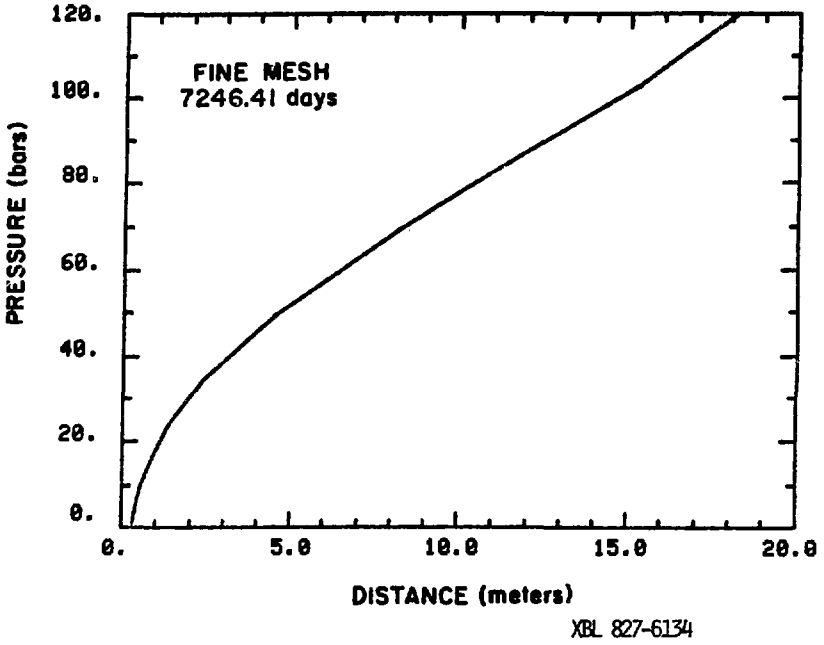

FIGURE A.7 Pressure vs. distance from center line of canisters after 20 years - reference case fine mesh (z = 10.1 m).

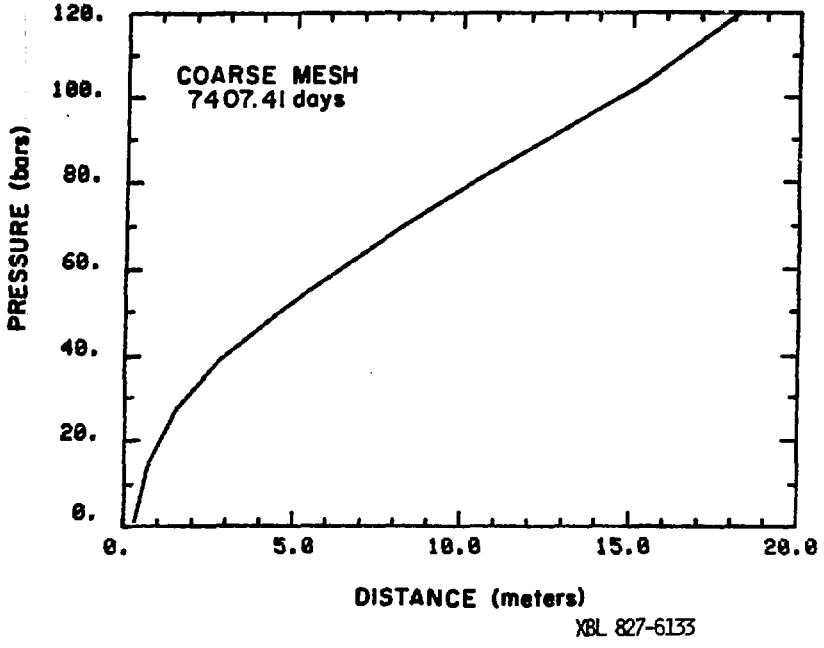

FIGURE A.8 Pressure vs. distance from center line of canisters after 20 years - refsrence case, coarse mesh (z = 10.1 m).

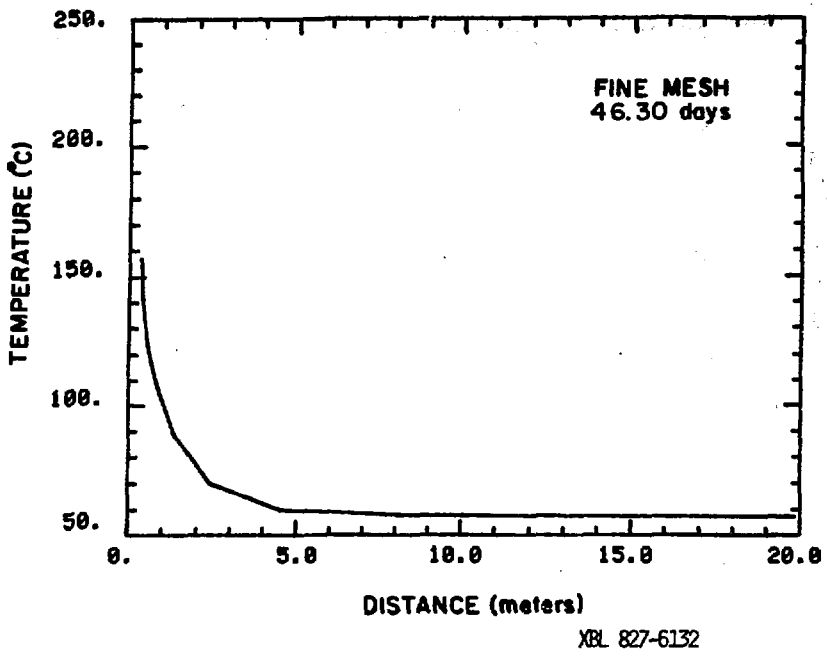

FIGURE A.9 Temperature vs. radial distance from centerline of canisters after 1.5 months - reference case fine mesh (z = 10.1 m).

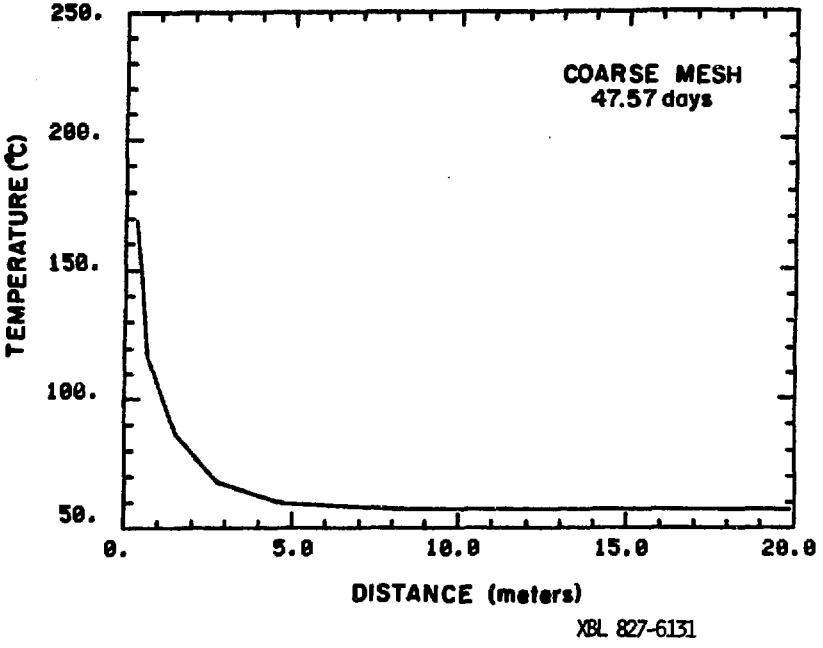

FIGURE A.10 Temperature vs. radial distance from centerline of canisters after 1.5 months - reference case coarse mesh (z = 10.1 m)

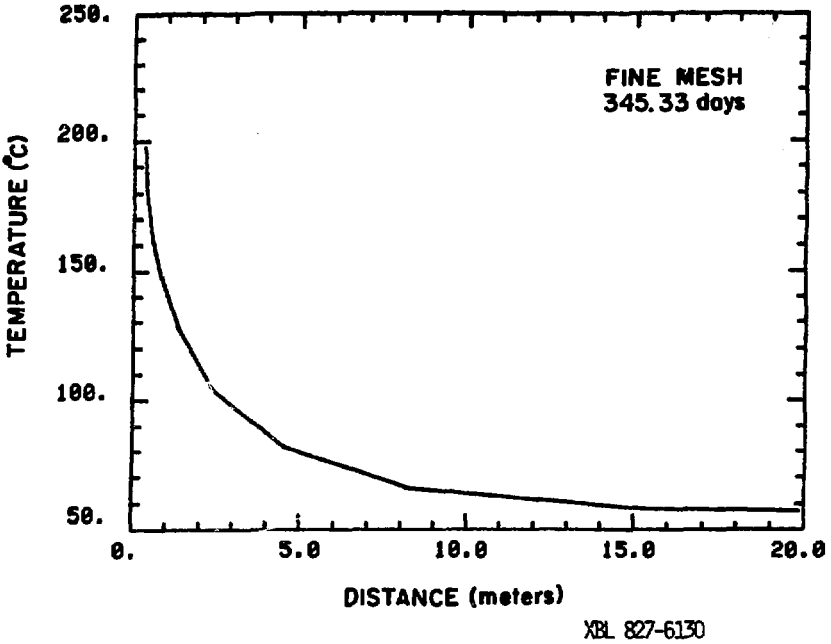

FIGURE A.11 Temperature vs. radial distance from centerline of canisters after 1 year - reference case fine mesh (z = 10.1 m).

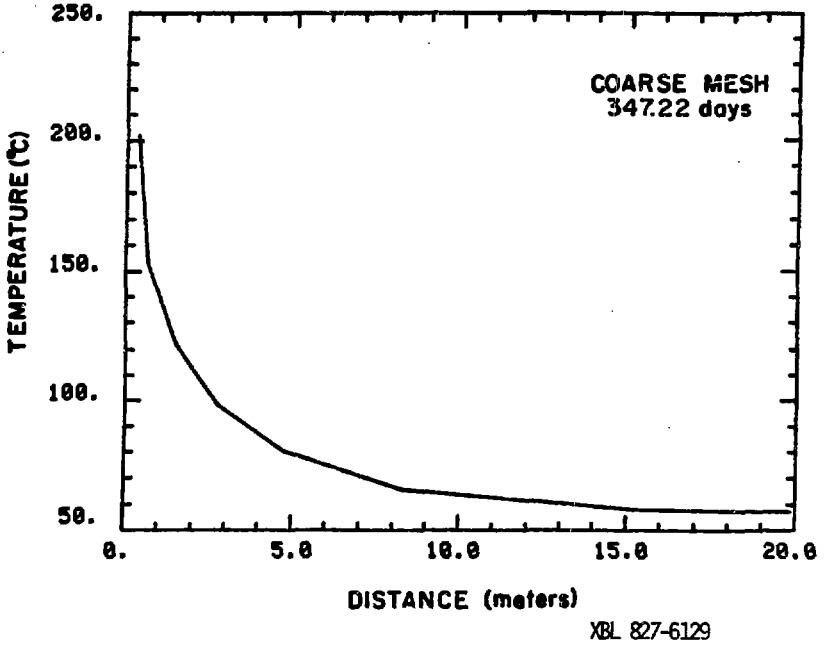

FIGURE A.12 Temperature vs. radial distance from centerline of canisters after 1 year - reference case coarse mesh (z = 10.1 m).

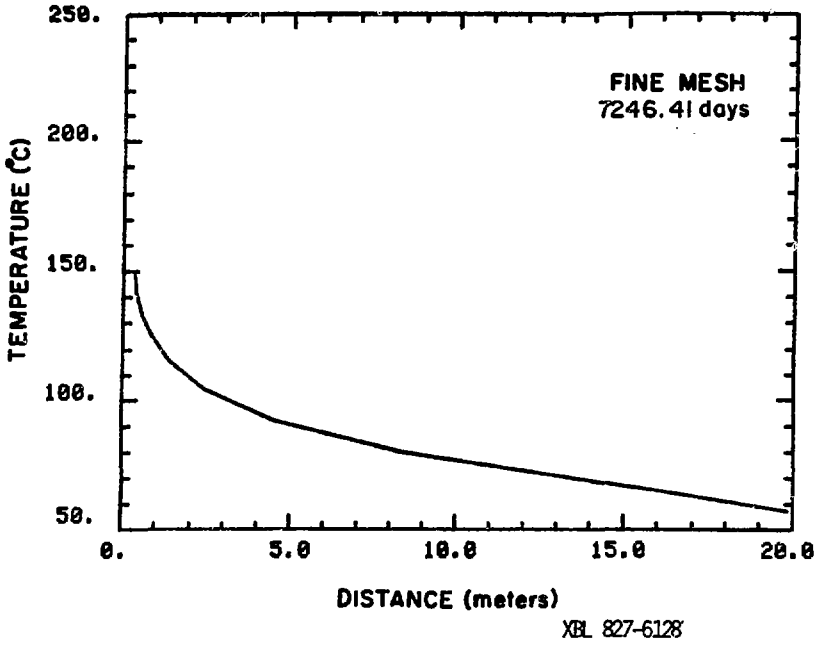

FIGURE A.13 Temperature vs. radial distance from centerline of canisters after 20 years - reference case fine mesh (z = 10.1 m).

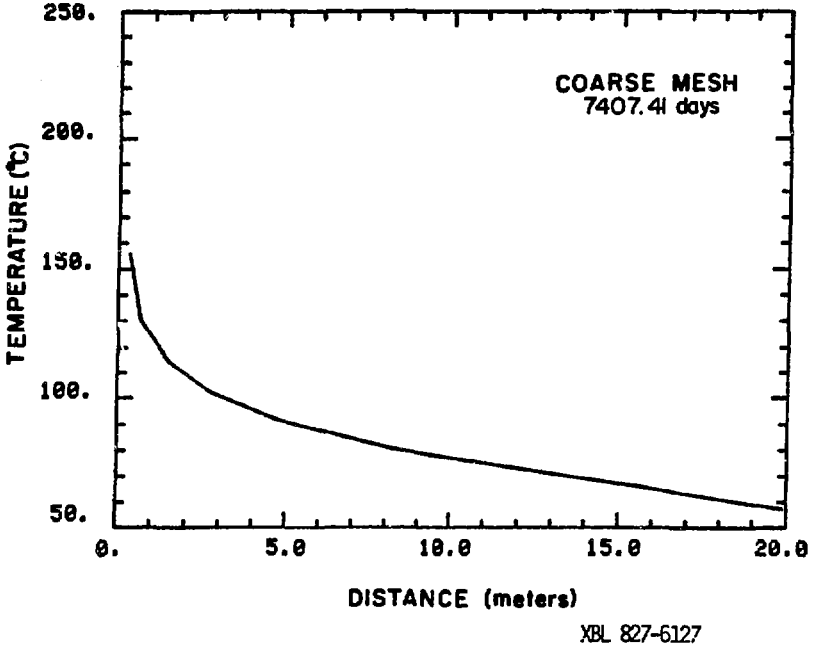

FIGURE A.14 Temperature vs. radial distance from centerline of canisters after 20 years - reference case coarse mesh (z = 10.1 m).

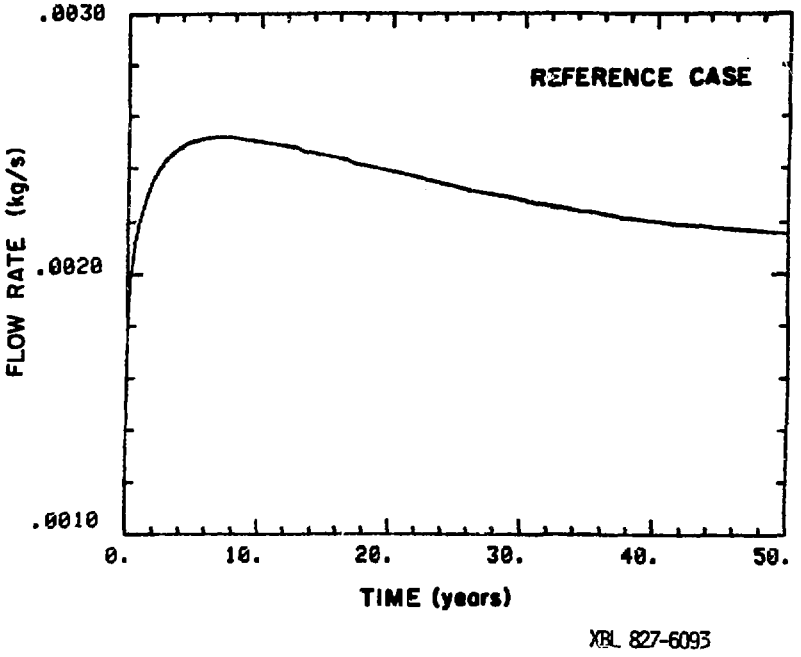

FIGURE A.15 Total fluid flow into storage tunnel - reference case.

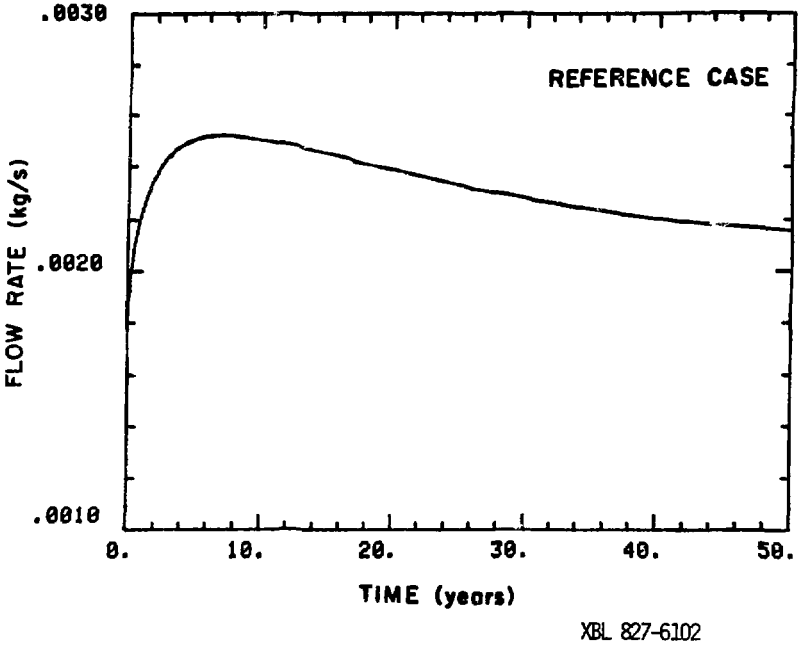

FIGURE A.16 Total fluid flow from boundary of model - reference case.

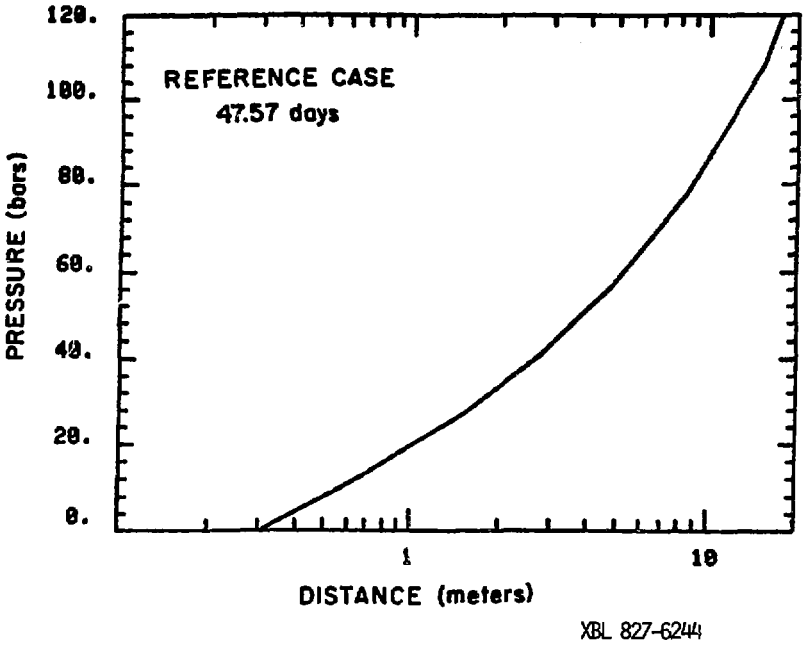

FIGURE A.17 Pressure vs. radial distance from centerline of canister after 1.5 months - reference case (z = 10.1 m).

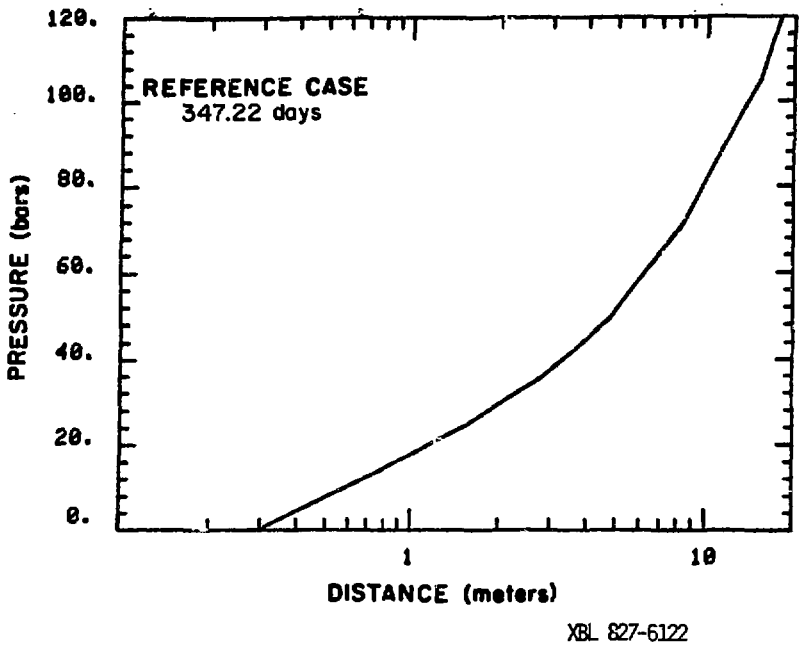

FIGURE A.13 Pressure vs. radial distance from centerline of canister after 1 year - reference case (z = 10.1 m).

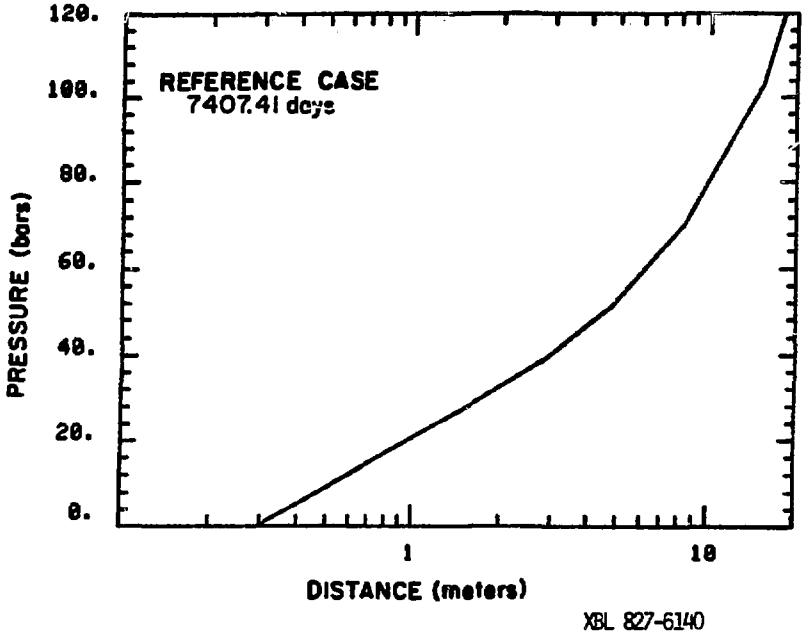

FIGURE A.19 Pressure vs. radial distance from centerline of canister after 20 years - reference case (z = 10.1 m).

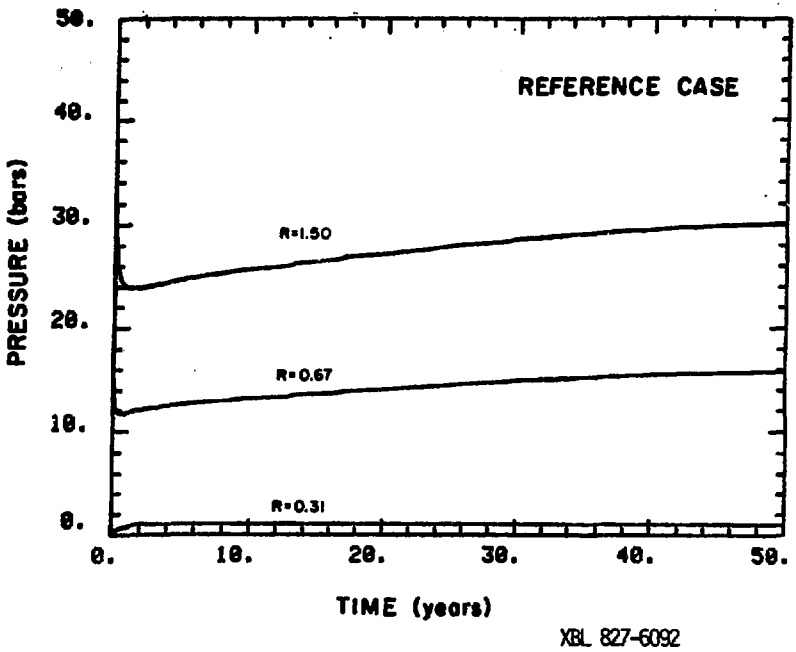

FIGURE A.20 Variations of pressures with time at selected points - reference case ($z = 10.1$ m).

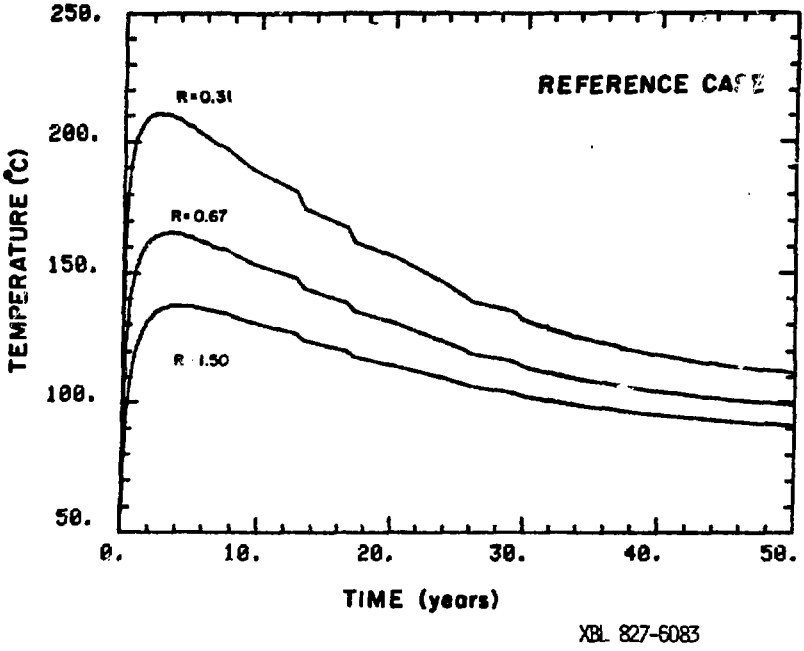

FIGURE A.21 Variations of temperatures with time at selected points - reference case (z = 10.1 m).

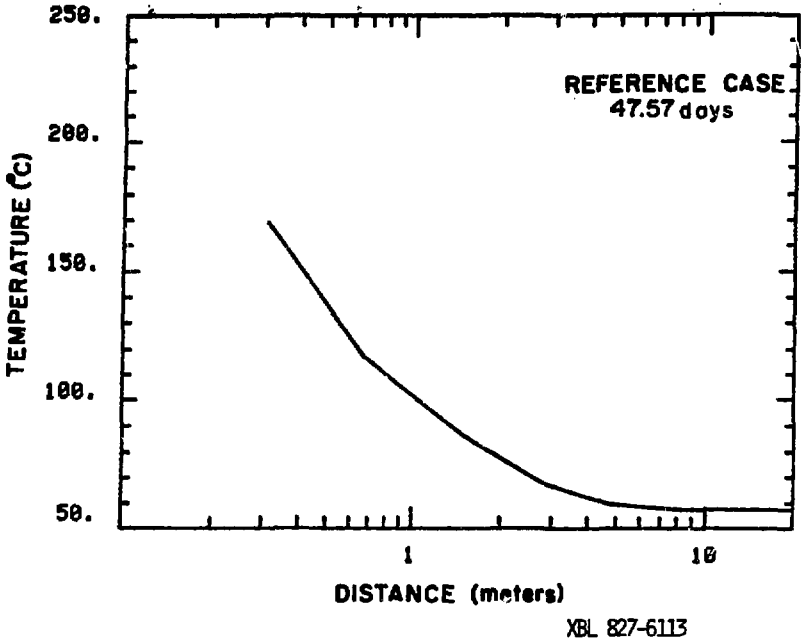

FIGURE A.22 Temperature vs. distance from center line of canister after 1.5 months - reference case (z = 10.1 m).

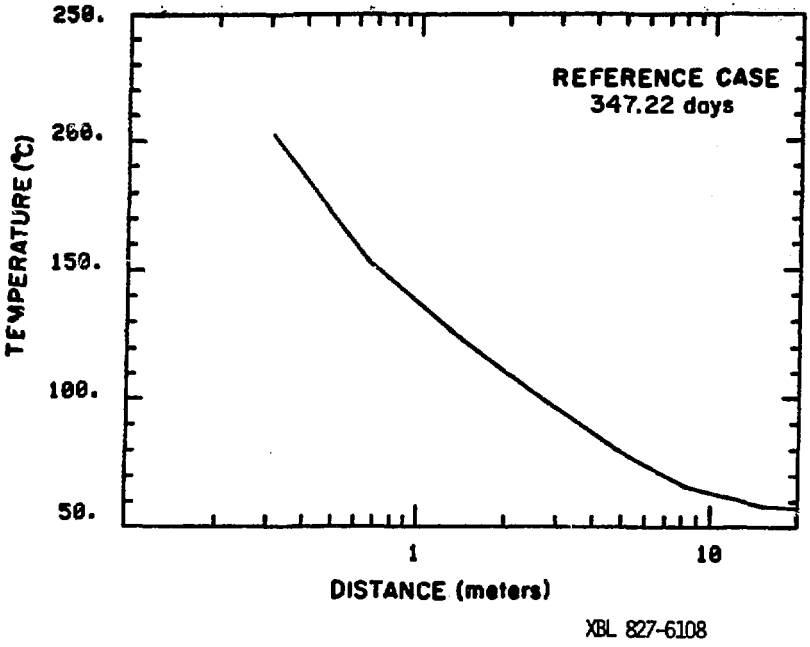

FIGURE A.23 Temperature vs. distance from centerline of canister after 1 year - reference case (z = 10.1 m).

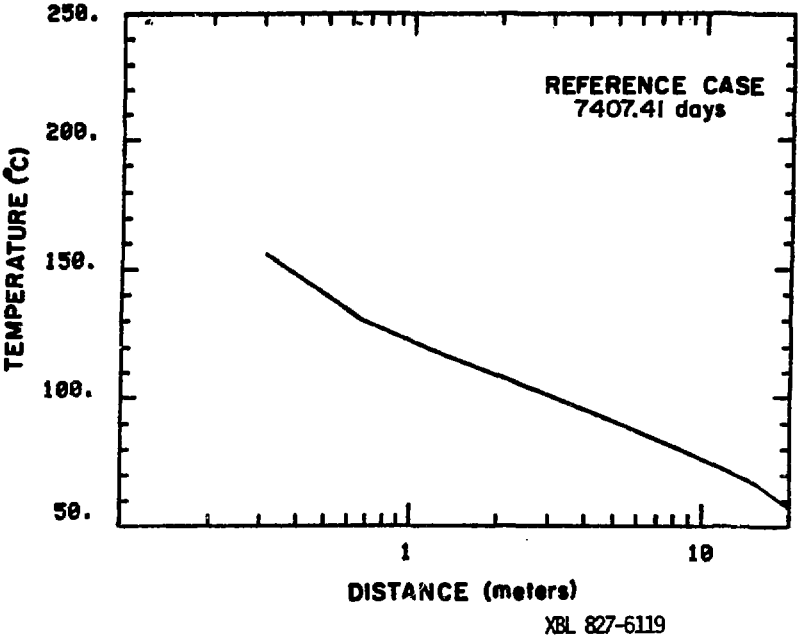

FIGURE A.24 Temperature vs. distance from centerline of canister ater 20 years - reference case (z = 10.1 m).

APPENDIX B

COMPUTER GENERATED PLOTS OF RESULTS OF SENSITIVITY STUDIES

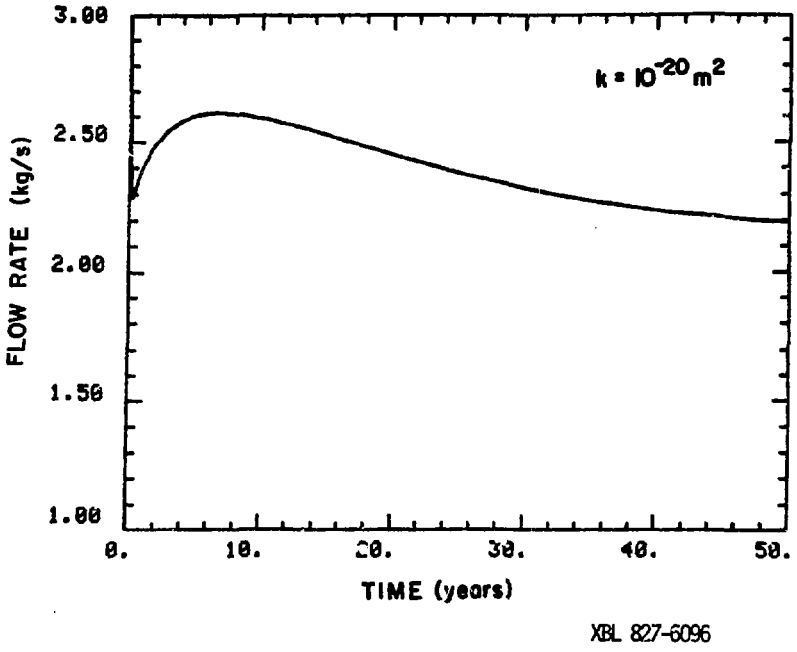

FIGURE B.1 Total fluid flow into storage tunnel - low permeability case.

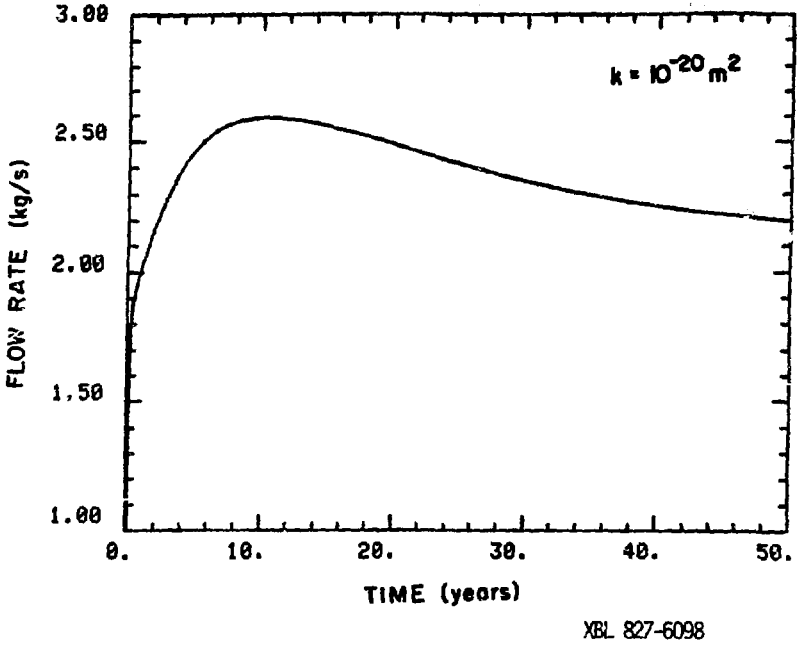

FIGURE B.2 Total fluid flow from boundary of model - low permeability case.

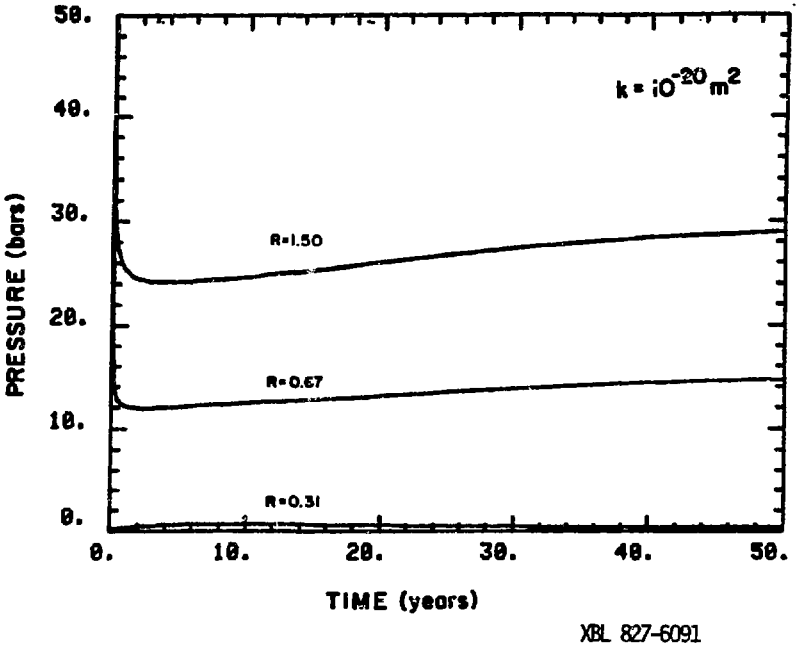

FIGURE B.3 Variations of pressure with time at selected points - low permeability case (z = 10.1 m).

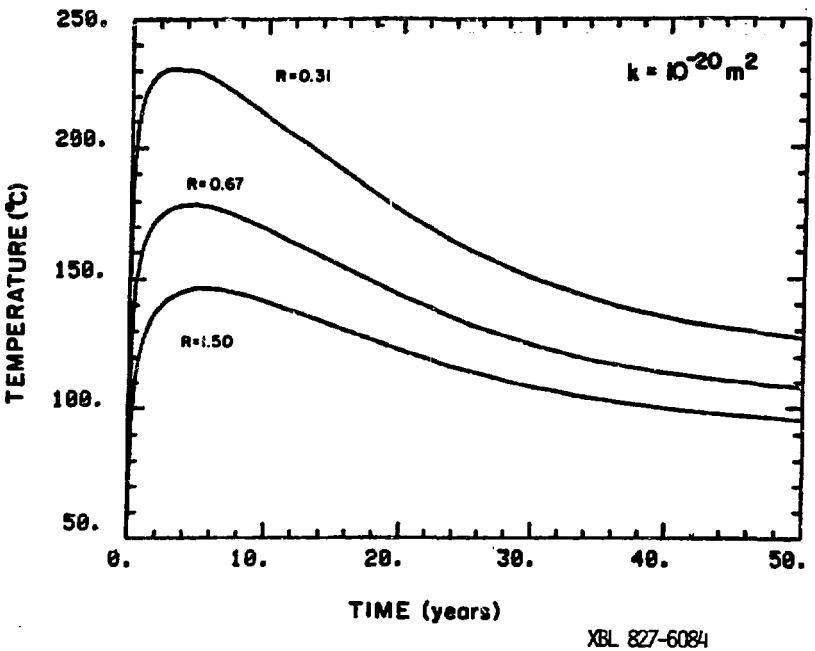

FIGURE B.4 Variation of temperature with time at selected points - low permeability case (z = 10.1 m).

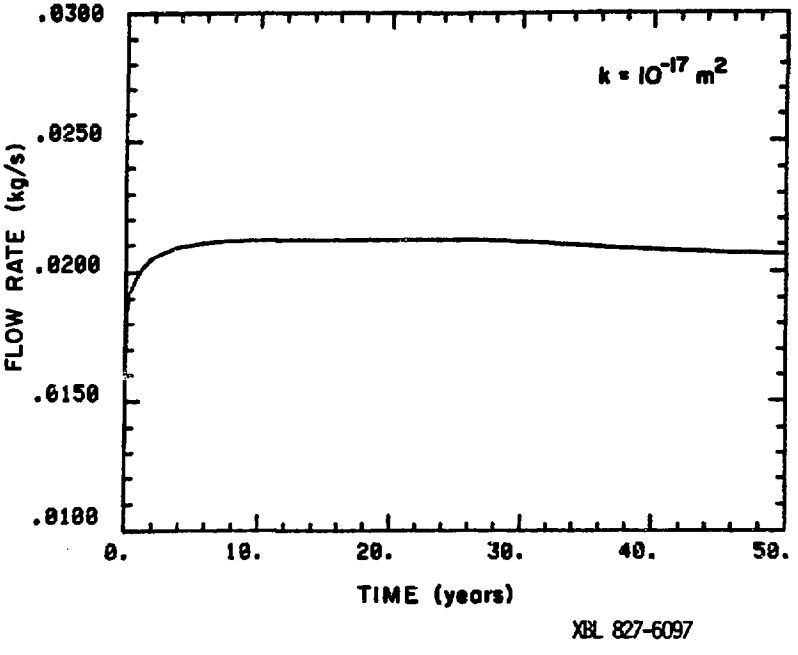

FIGURE B.5 Total fluid flow into storage tunnel - high permeability case.

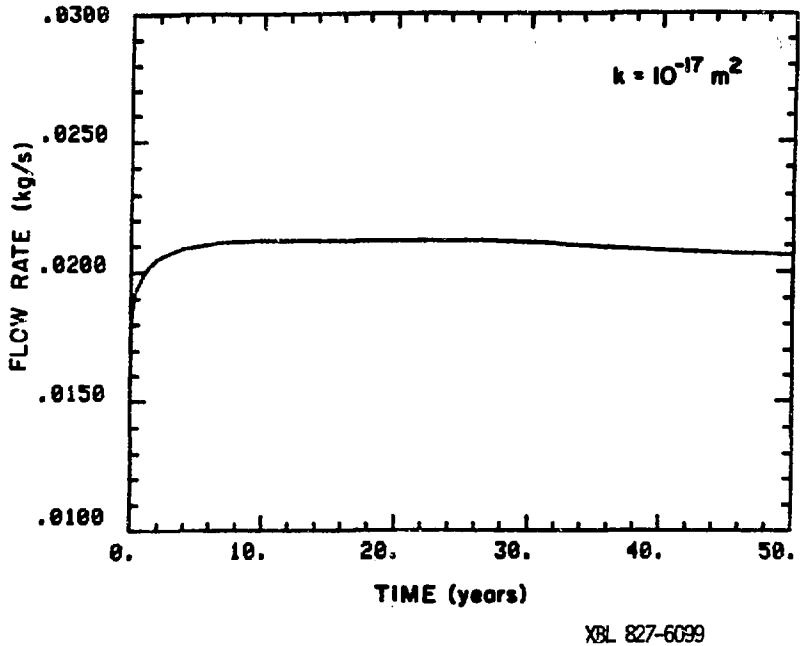

FIGURE B.6 Total fluid flow from boundary of model - high permeability case.

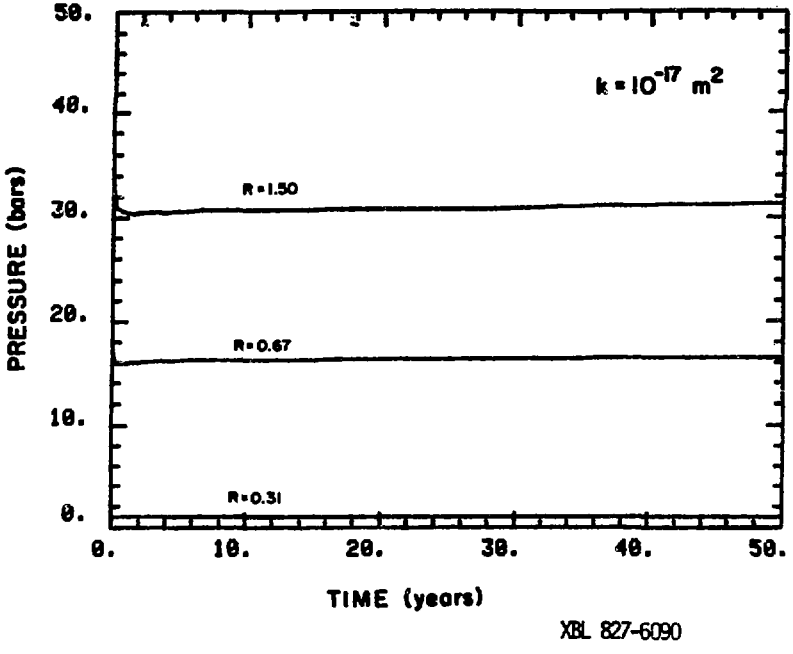

FIGURE B.7 Variations of pressure with time at selected points - high permeability case (z = 10.1 m).

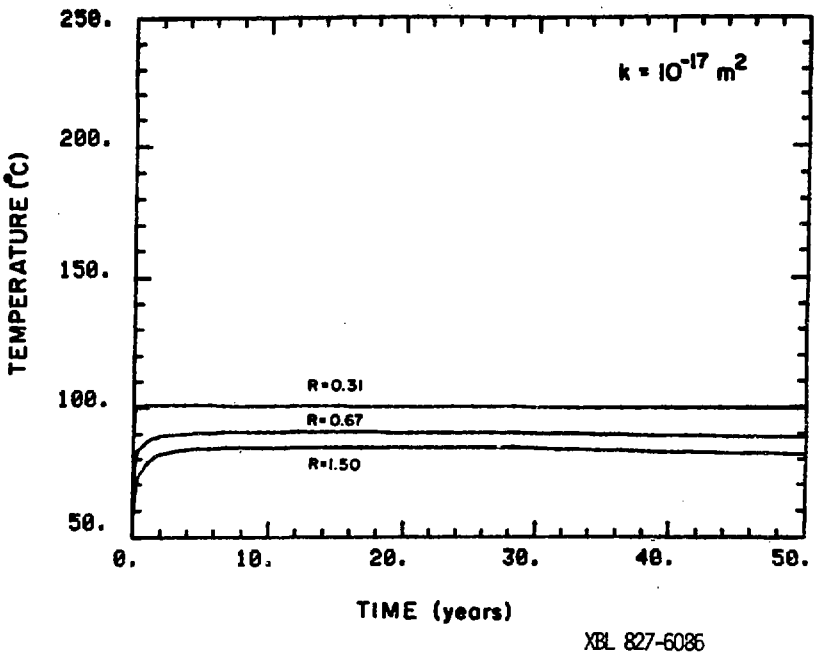

FIGURE B.8 Variations of temperature with time at selected points - high permeability case (z = 10.1 m).

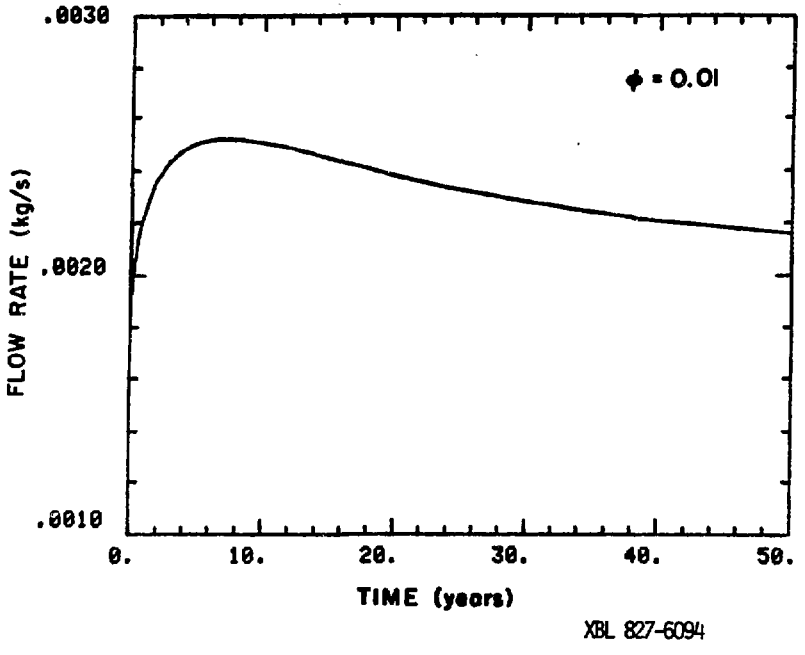

FIGURE B.9 Total fluid flow into storage tunnel - large porosity case.

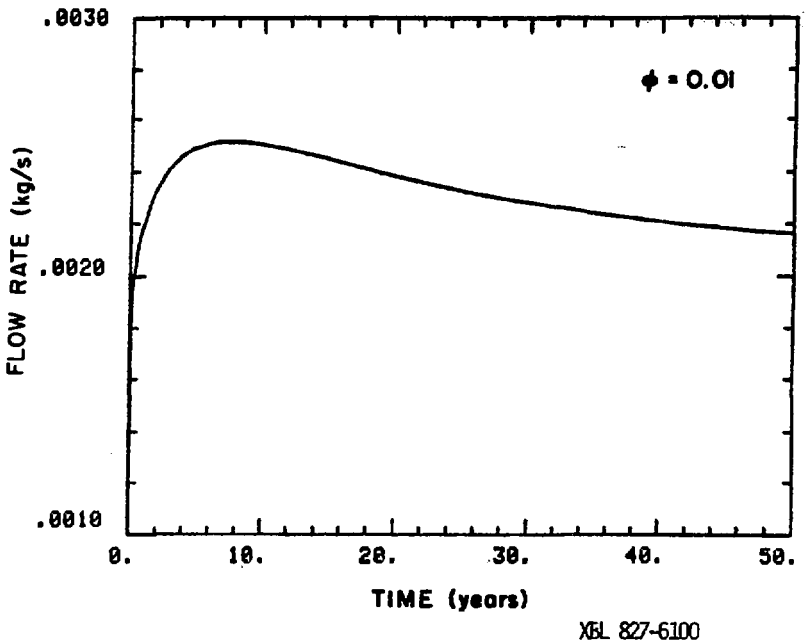

FIGURE B.10 Total fluid flow from boundary of model - large porosity case.

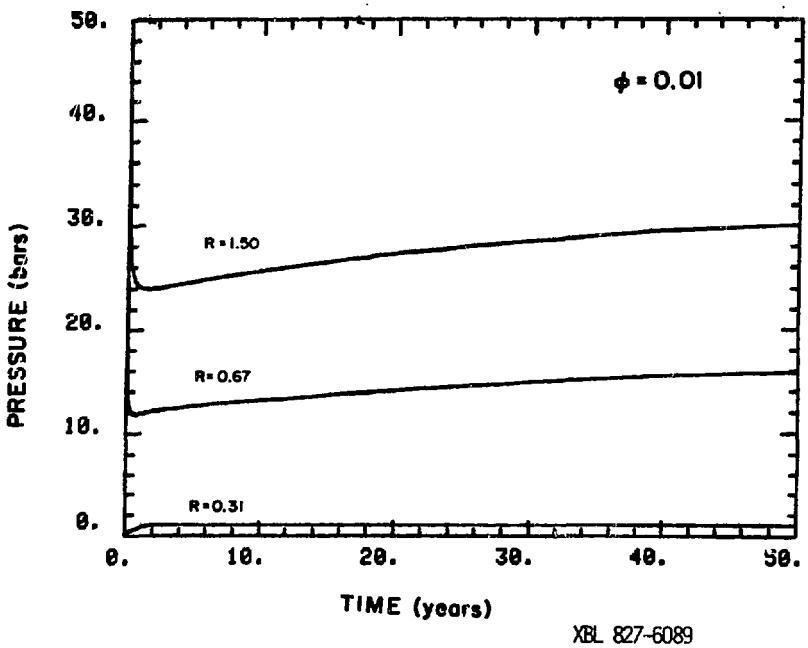

FIGURE B.11 Variations of pressure with time at selected points - large porosity case (z = 10.1 m).

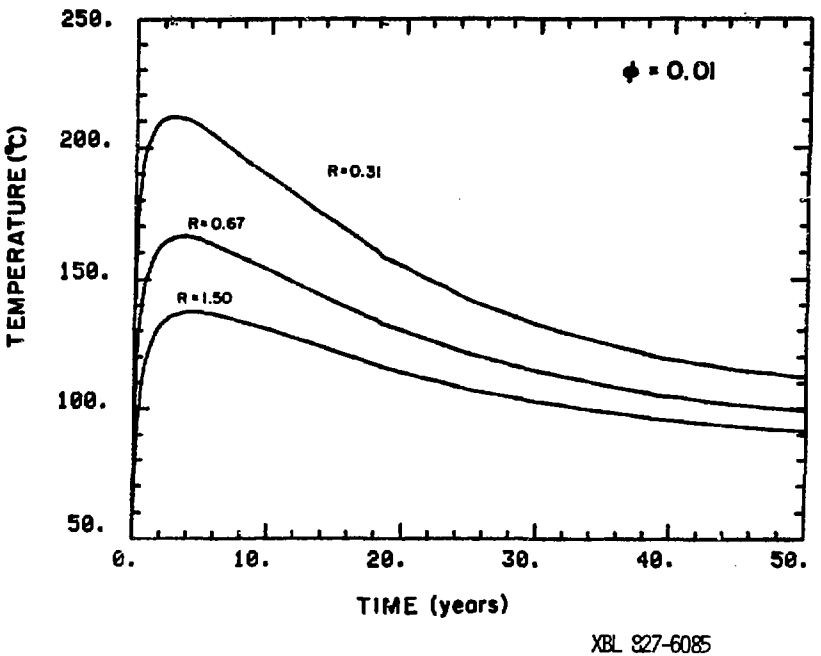

FIGURE B.12 Variations of temperature with time at selected points - large porosity case (z = 10.1 m).

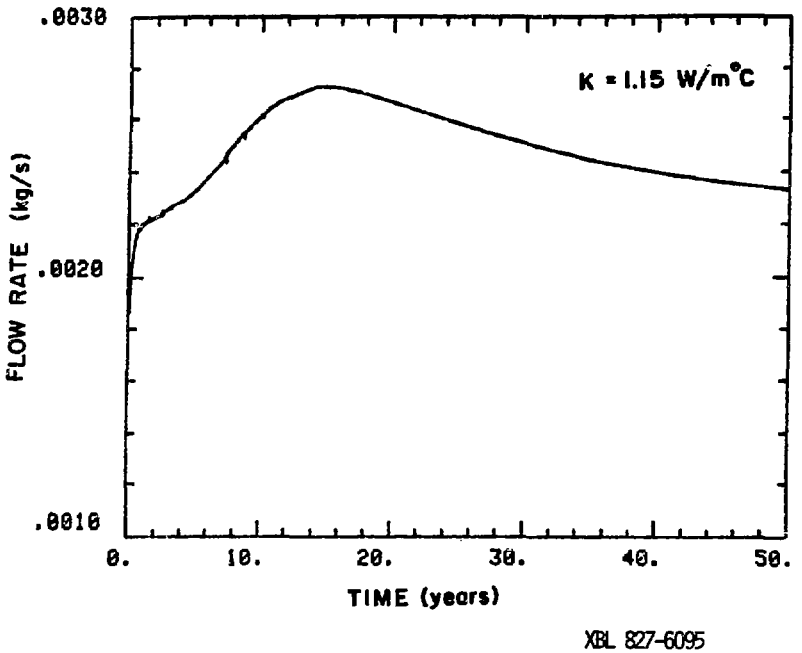

FIGURE B.13 Total fluid flow into storage tunnel - low heat conductivity case.

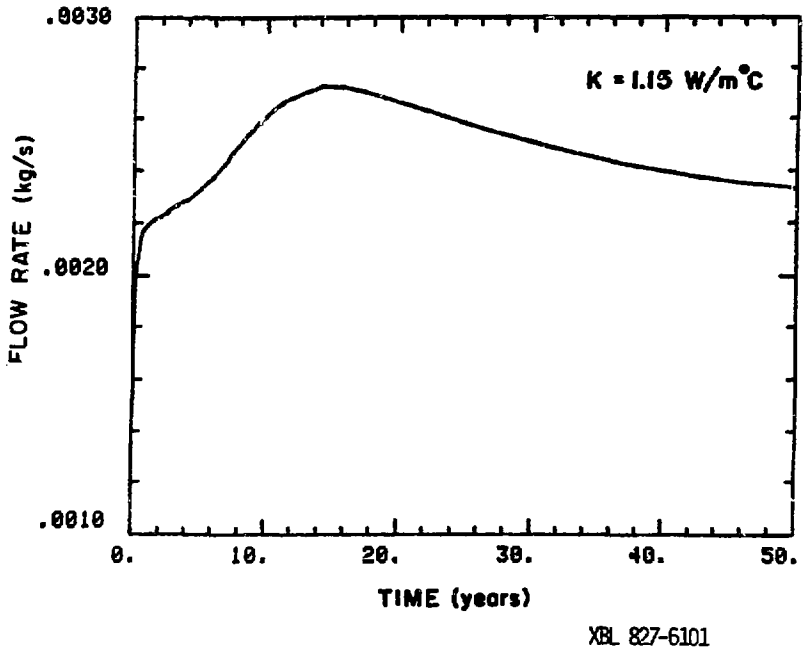

FIGURE B.14 Total fluid flow from boundary of model - low heat conductivity case.

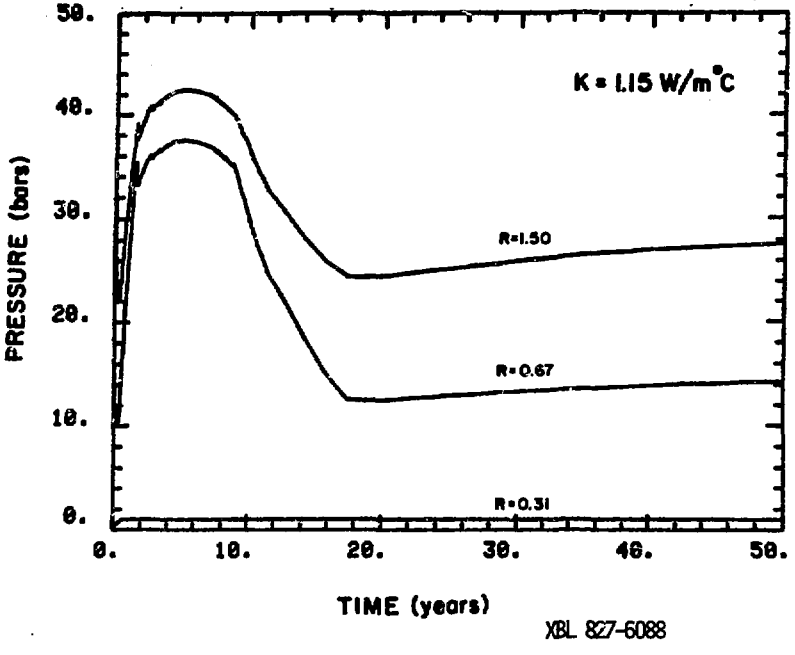

FIGURE B.15 Variations of pressure with time at selected points - low heat conductivity case (z = 10.1 m).

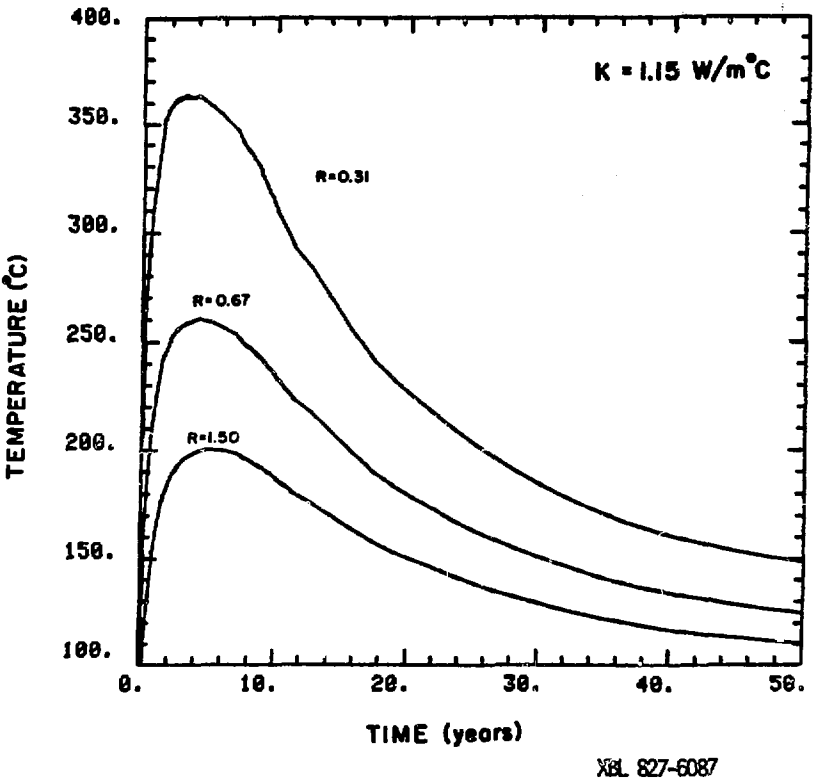

FIGURE B.16 Variations of temperature with time at selected points - low heat conductivity case (z = 10.1 m).

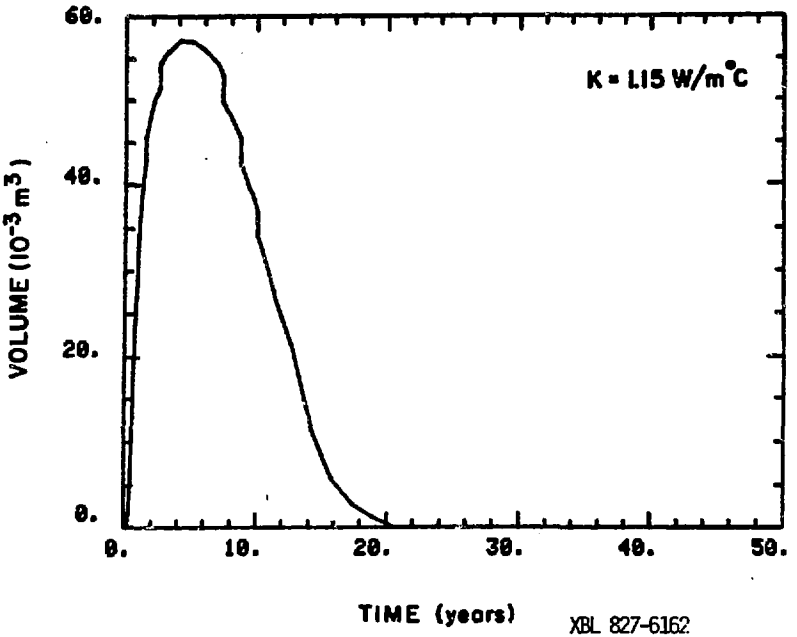

FIGURE B.17 Volume of steam in rock mass - low heat conductivity case.

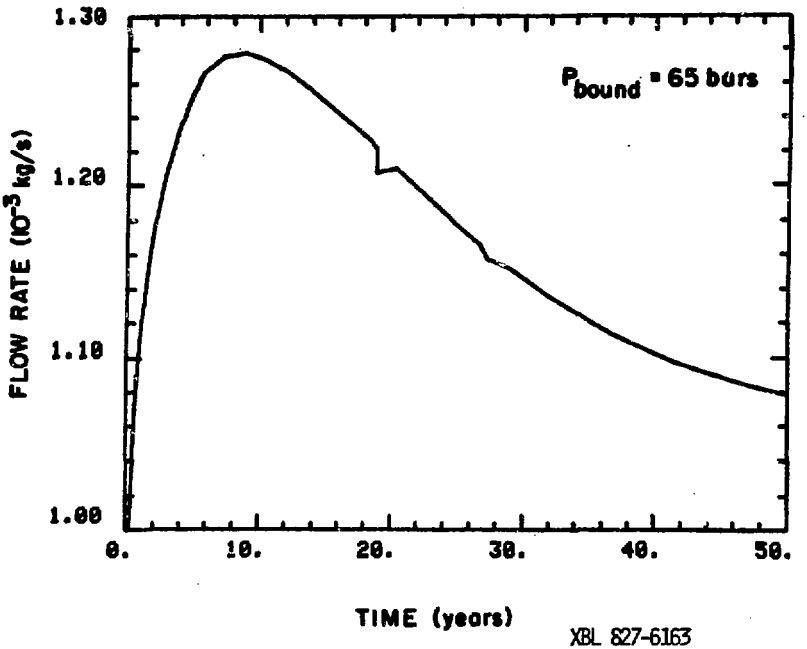

FIGURE B.18 Total fluid flow in storage tunnel - low boundary pressure case.

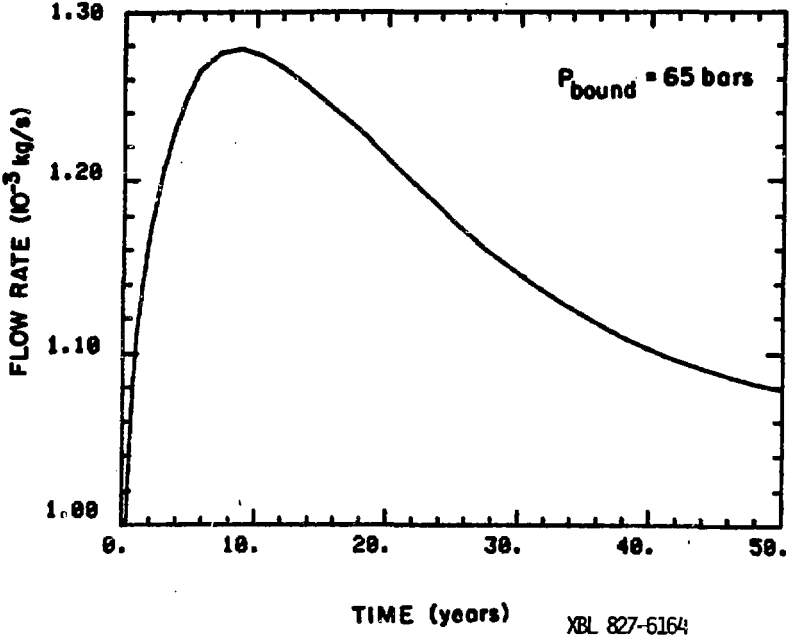

FIGURE B.19 Total fluid flow from boundary of model - low boundary pressure case.

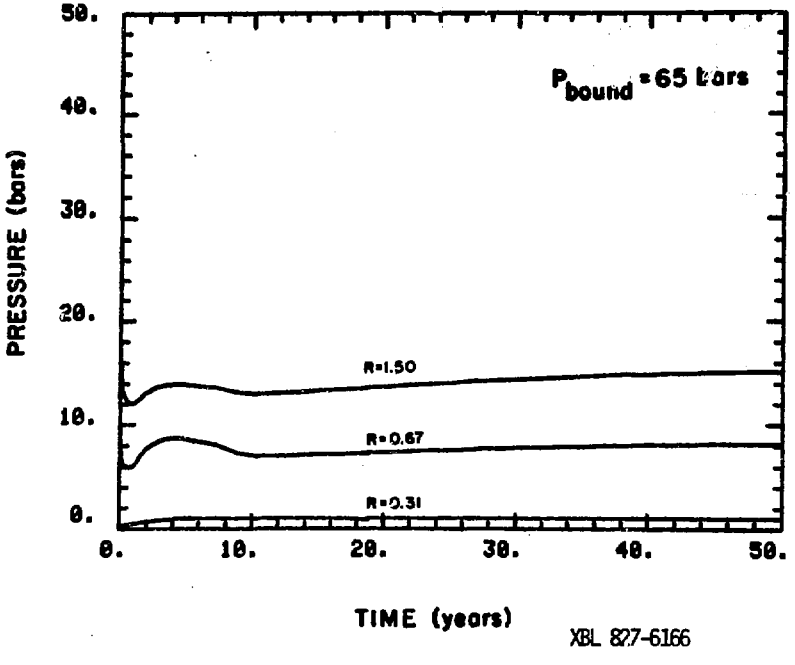

FIGURE B.20 Variations of pressure with time at selected points - low boundary pressure case (z = 10.1 m).

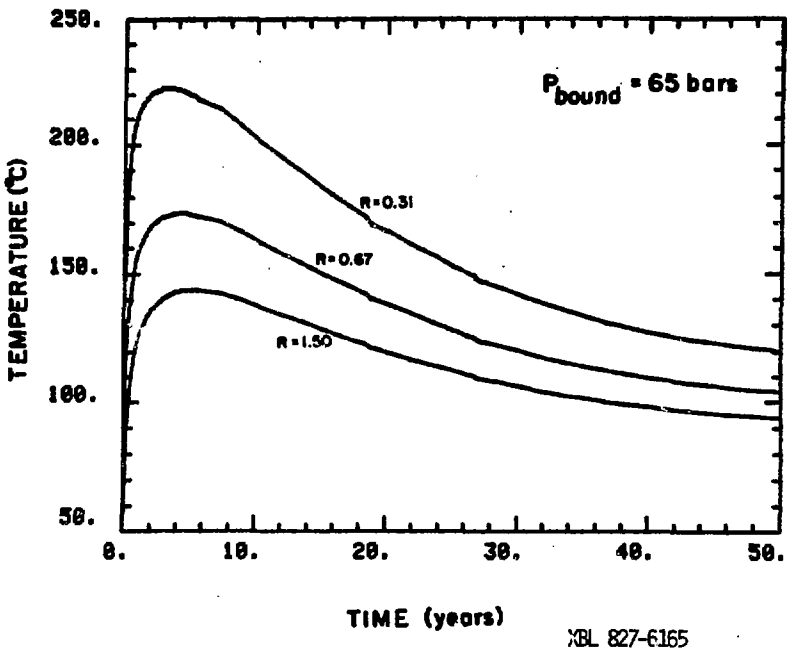

FIGURE B.21 Variations of temperature with time at selected points - low boundary pressure case (z = 10.1 m).

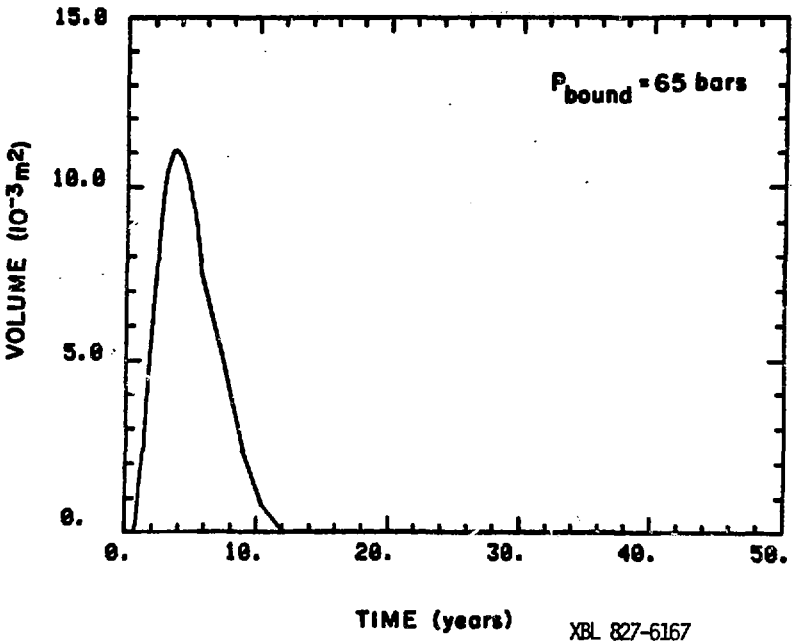

FIGURE B.22 Volume of steam in rock mass - low boundary pressure case.

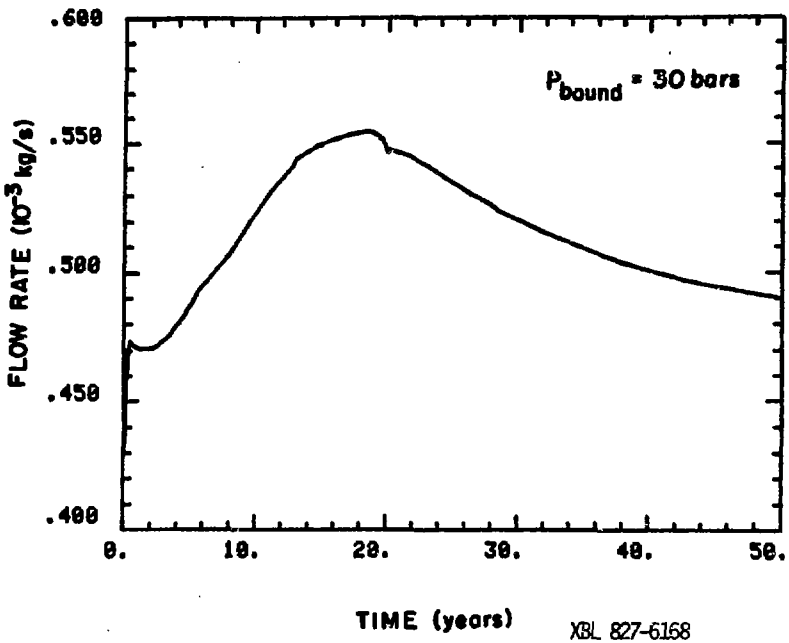

FIGURE B.23 Total fluid flow into storage room - very low boundary pressure case.

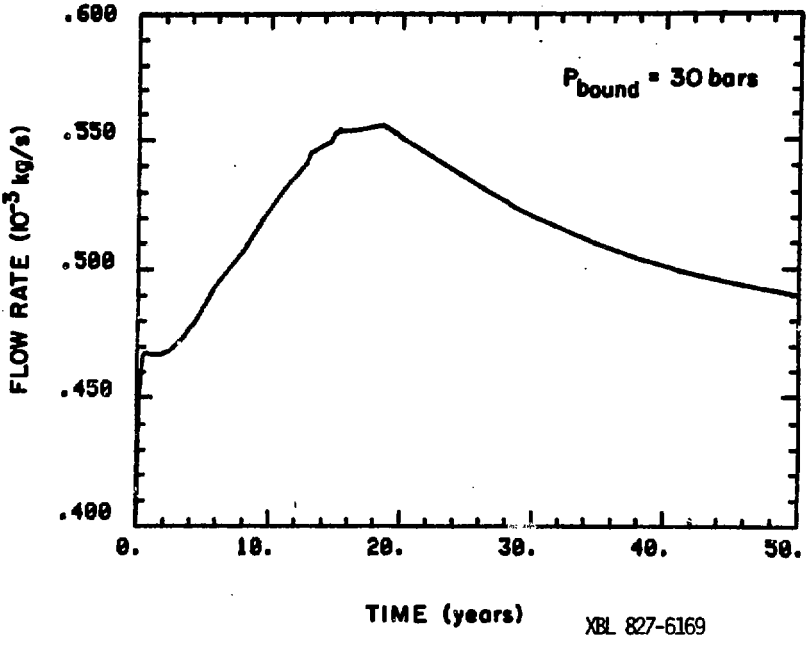

FIGURE B.24 Total fluid flow from boundary of model - very low boundary pressure case.

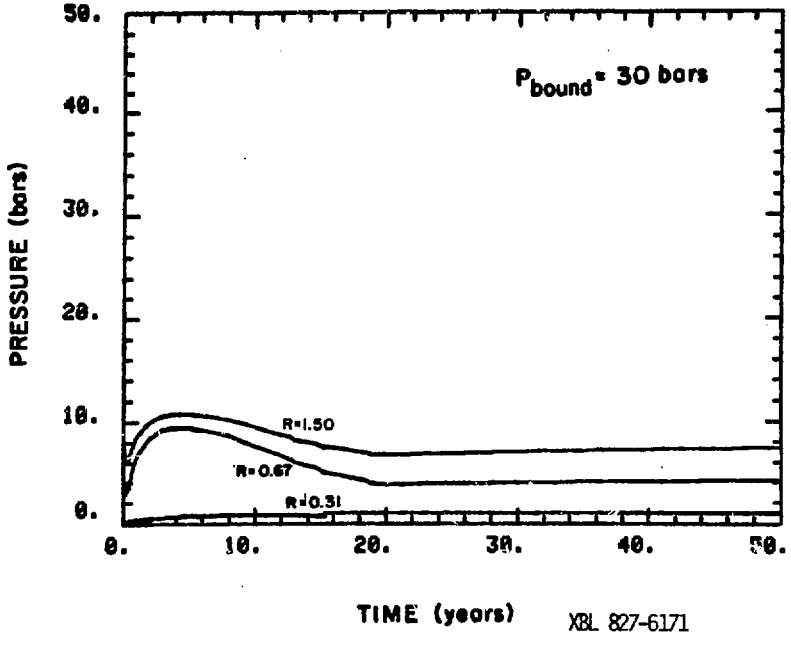

FIGURE B.25 Variation of pressure with time at selected points - very low boundary pressure case (z = 10.1 m).

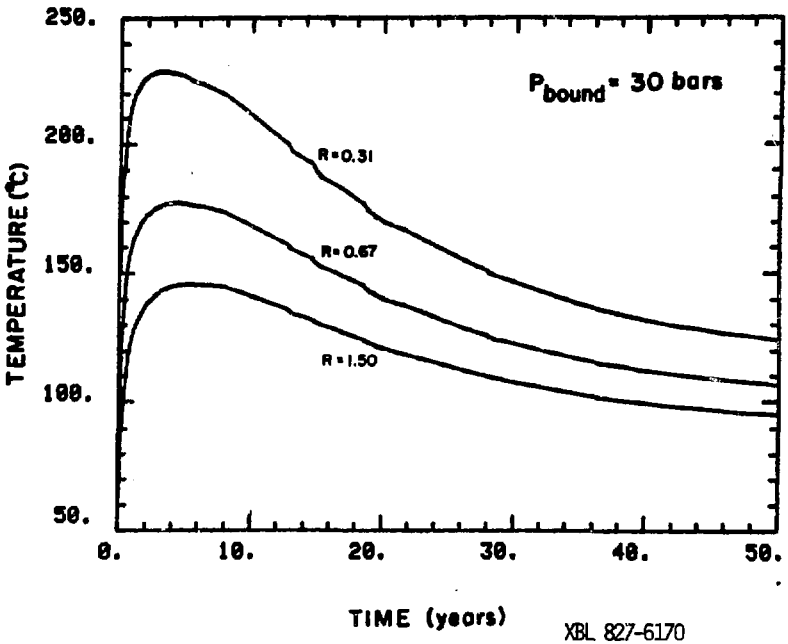

FIGURE B.26 Variations of temperature with time at selected points - very low boundary pressure case (z = 10.1 m).

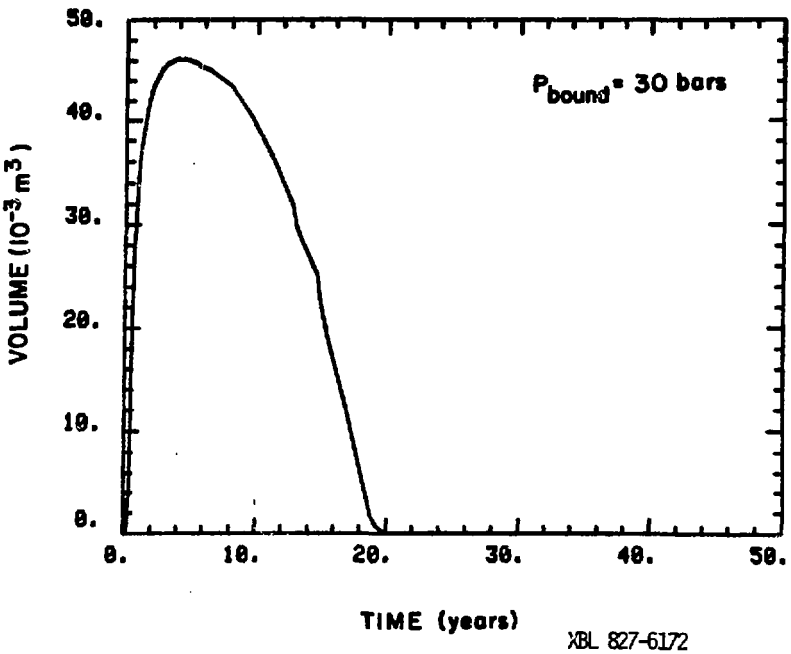

FIGURE B.27 Volume of steam in rock mass - very low boundary pressure case.

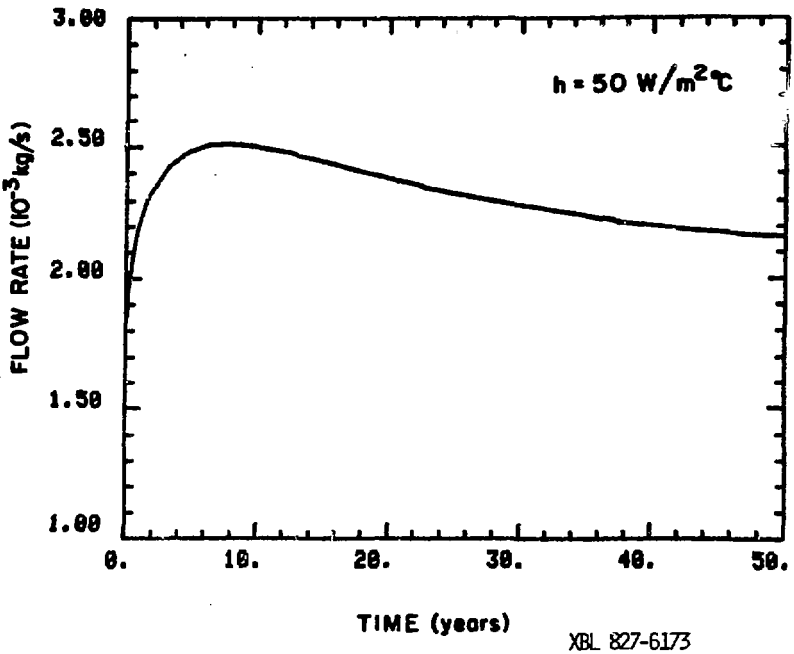

FIGURE B.28 Total fluid flow into storage tunnel - large heat transfer coefficient case.

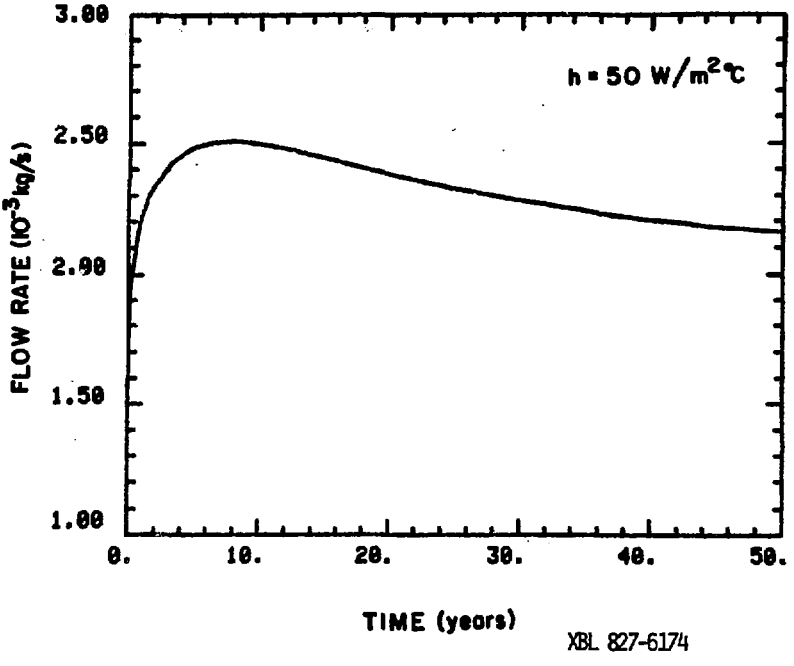

FIGURE B.29 Total flow from boundary of model - large heat transfer coefficient case.

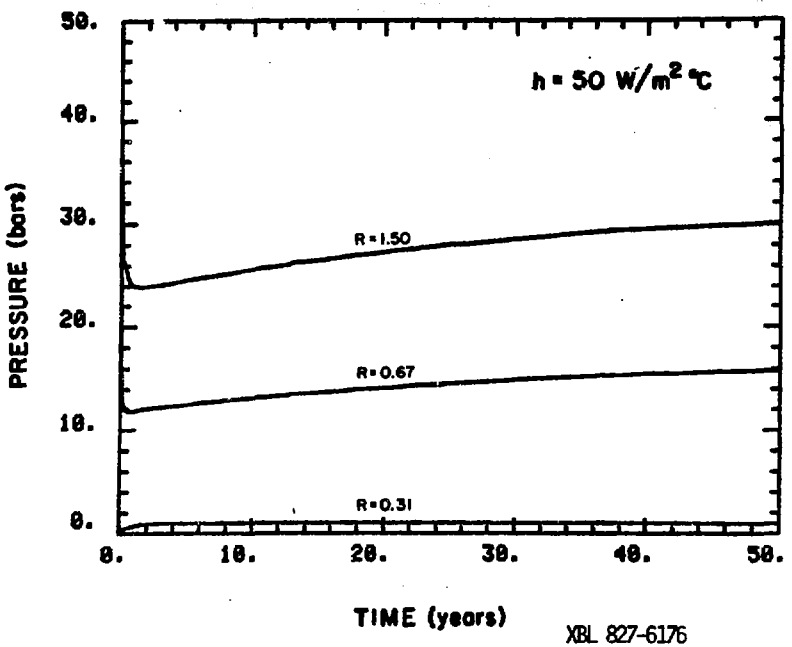

FIGURE B.30 Variations of pressure with time at selected points - large heat transfer coefficient case (z = 10.1 m).

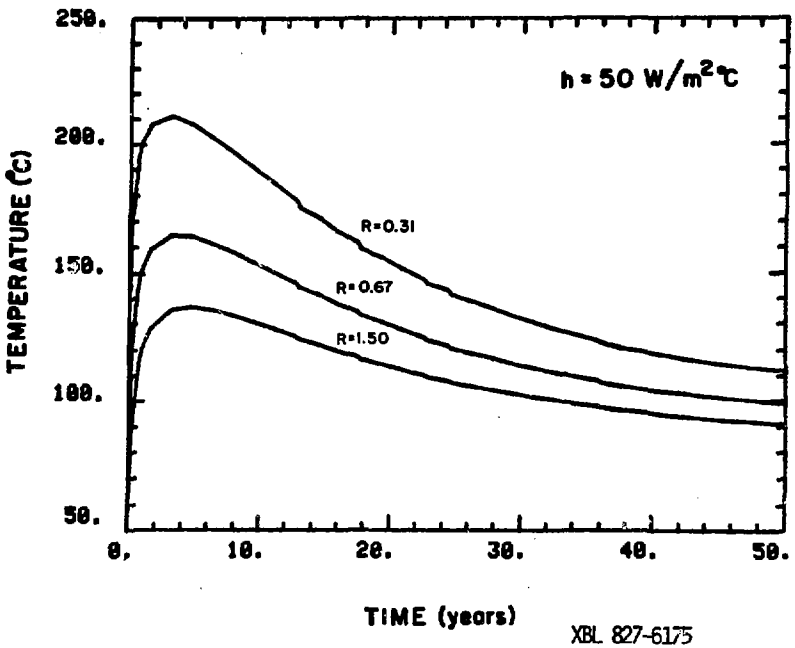

FIGURE B.31 Variations of temperature with time at selected points - large heat transfer coefficient case (z = 10.1 m).

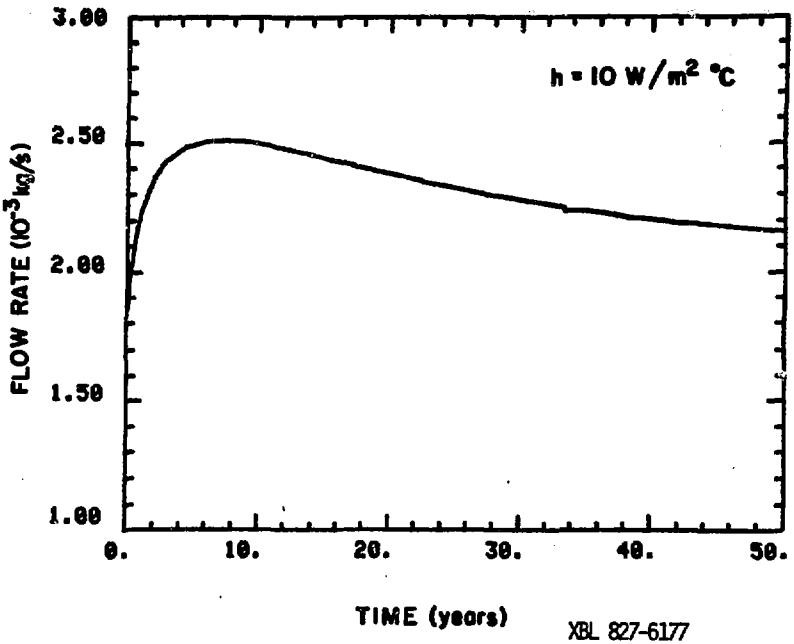

FIGURE B.32 Total fluid flow into storage tunnel - small heat transfer coefficient case.

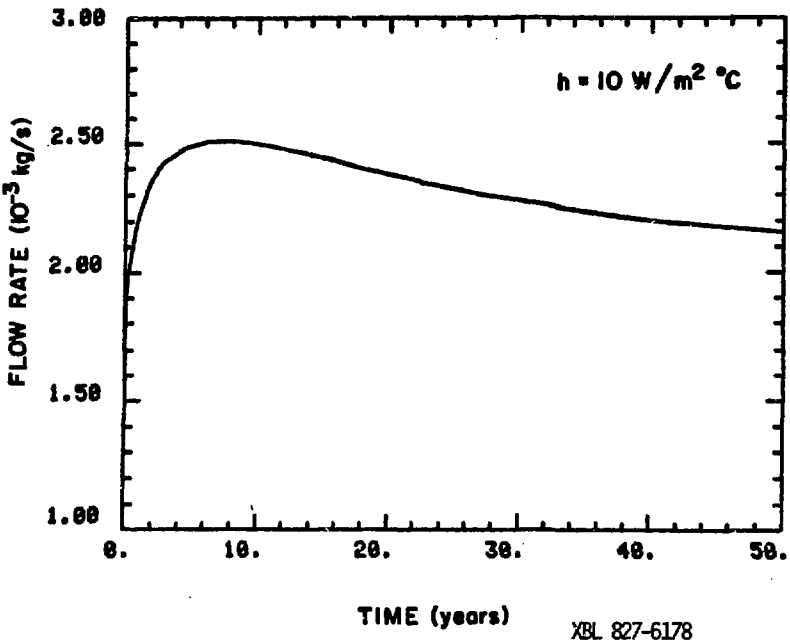

FIGURE B.33 Total fluid flow from boundary of model - small heat transfer coefficient case.

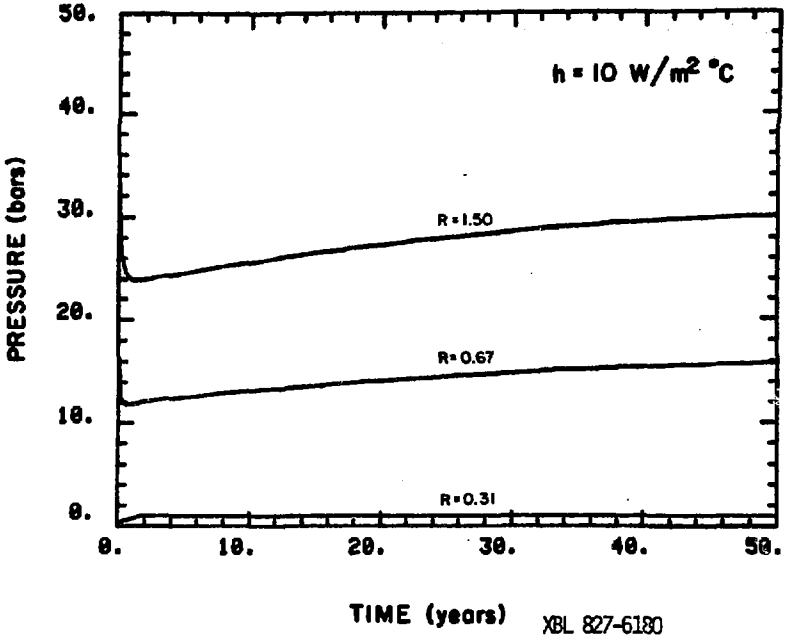

FIGURE B.34 Variations of pressure with time at selected points - small heat transfer coefficient case (z = 10.1 m).

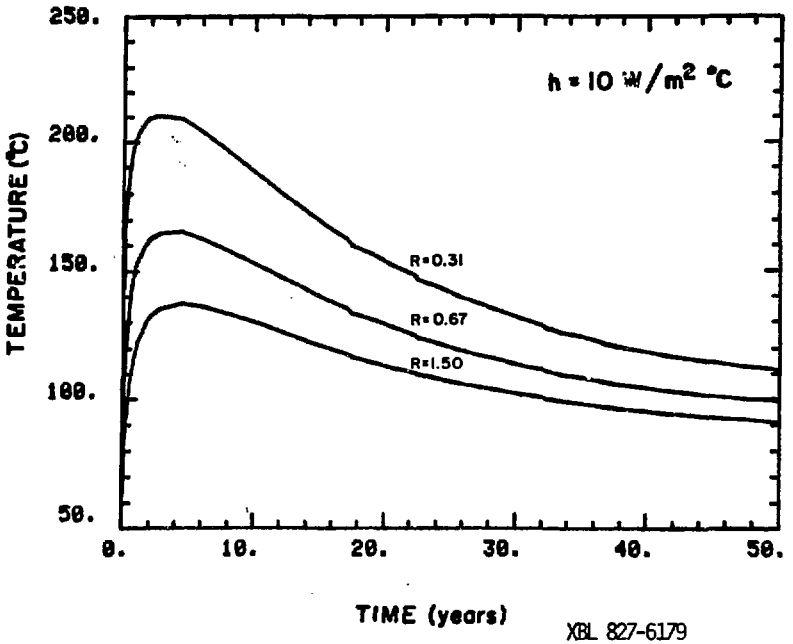

FIGURE B.35 Variations of temperature with time at selected points - small heat transfer coefficient case (z = 10.1 m).

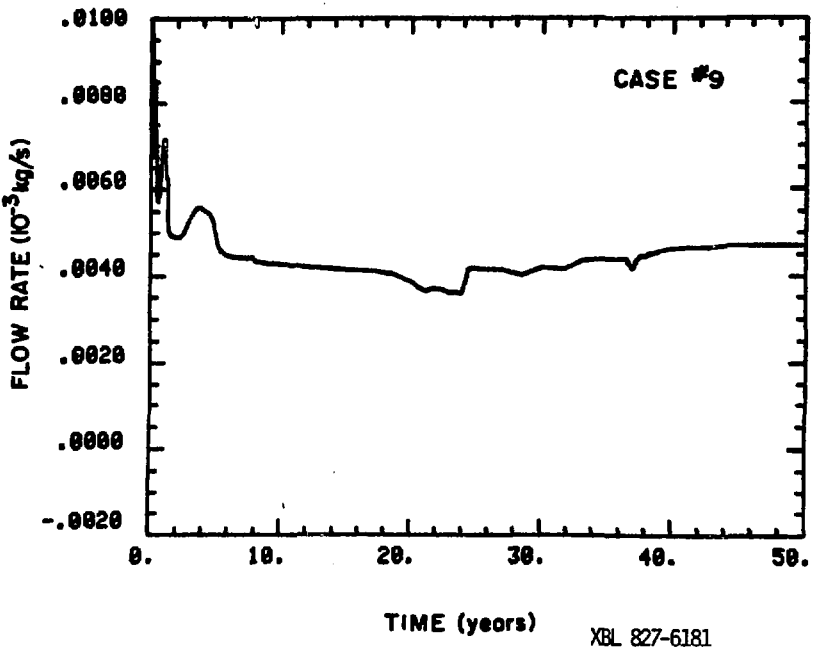

FIGURE B.36 Total fluid flow into storage tunnel - extreme case.

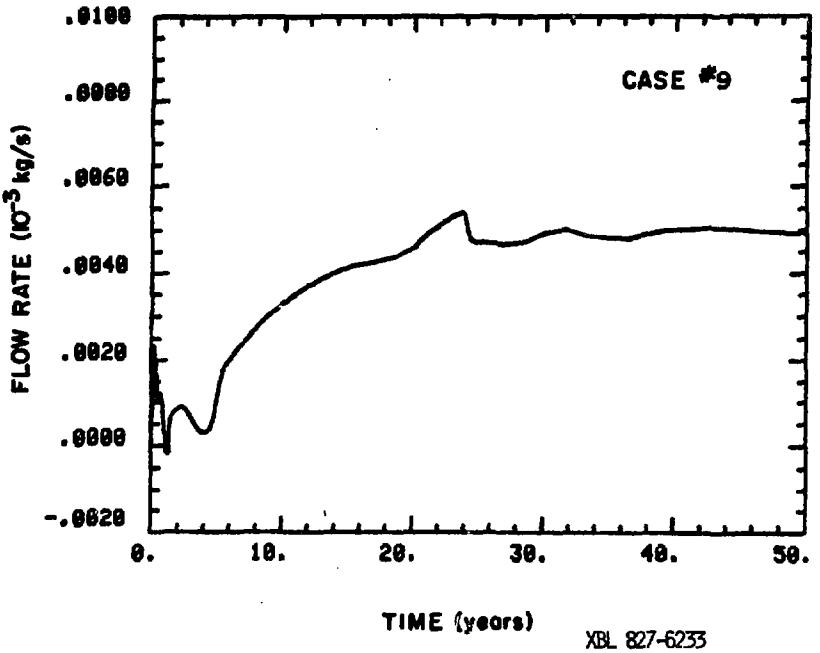

FIGURE B.37 Total fluid flow from boundary of model - extreme case.

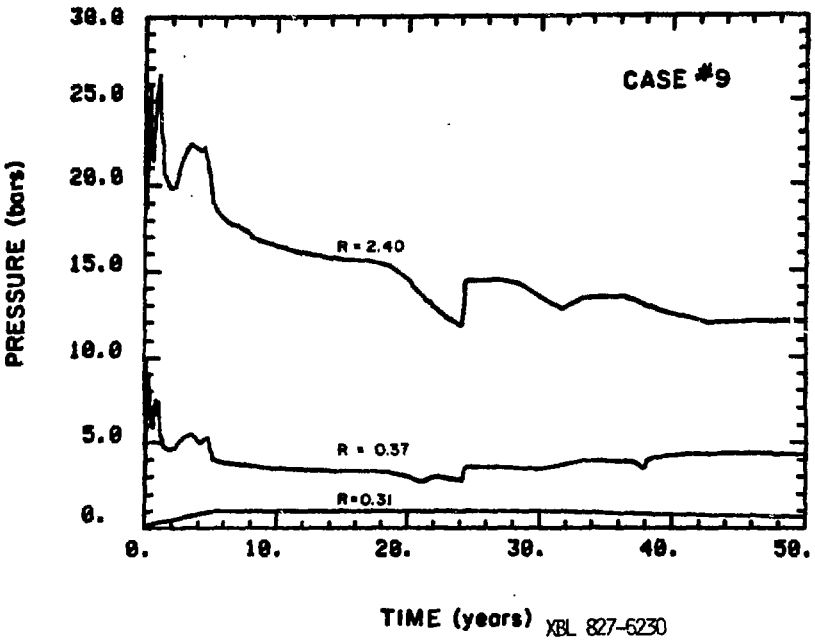

FIGURE B.38 Variations of pressure with time at selected points - extreme case (z = 10.1 m).

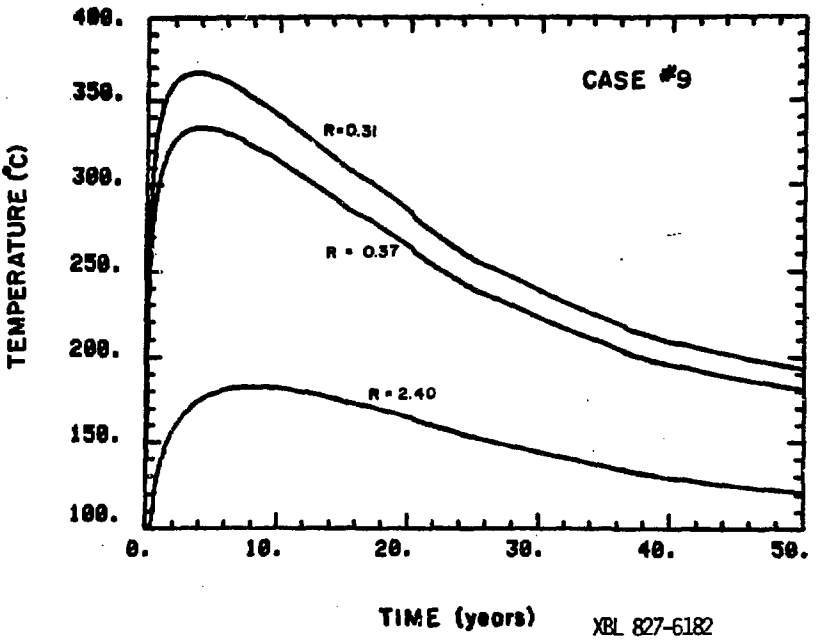

FIGURE B.39 Variations of temperature with time at selected points - extreme case (z = 10.1 m).

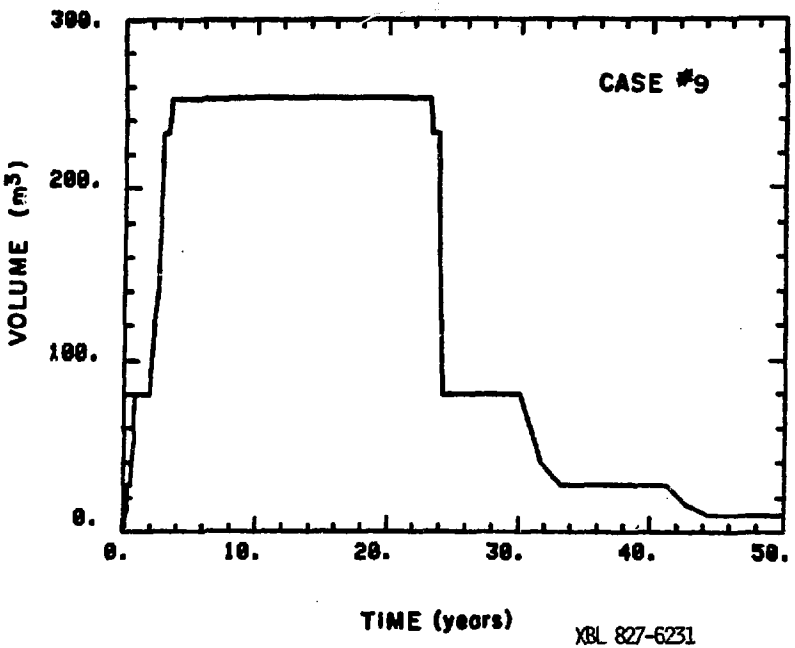

FIGURE B.40 Volume of rock mass in which boiling occurs - extreme case.